6-9-2009

Effect of Advanced Synthetically Enhanced Detector Resolution Algorithm on Specificity and Sensitivity of Portable High Purity Germanium Gamma Detector Spectra

LaTosha M. Bell

EFFECT OF ADVANCED SYNTHETICALLY ENHANCED DETECTOR RESOLUTION ALGORITHM ON SPECIFICITY AND SENSITIVITY OF PORTABLE HIGH PURITY GERMANIUM GAMMA DETECTOR SPECTRA

THESIS

LaTosha M. Bell

AFIT/GNE/ENP/09-J01

DEPARTMENT OF THE AIR FORCE
AIR UNIVERSITY

AIR FORCE INSTITUTE OF TECHNOLOGY

Wright-Patterson Air Force Base, Ohio

The views expressed in this thesis are those of the author and do not reflect the official policy or position of the United States Air Force, Department of Defense, or the United States Government.

AFIT/GNE/ENP/09-J01

EFFECT OF ADVANCED SYNTHETICALLY ENHANCED DETECTOR RESOLUTION ALGORITHM ON SPECIFICITY AND SENSITIVITY OF PORTABLE HIGH PURITY GERMANIUM GAMMA DETECTOR SPECTRA

THESIS

Presented to the Faculty

Department of Engineering Physics

Graduate School of Engineering and Management

Air Force Institute of Technology

Air University

Air Education and Training Command

In Partial Fulfillment of the Requirements for the

Degree of Master of Science in Nuclear Engineering

LaTosha M. Bell, BS

June 2009

APPROVED FOR PUBLIC RELEASE; DISTRIBUTION UNLIMITED

AFIT/GNE/ENP/09-J01

EFFECT OF ADVANCED SYNTHETICALLY ENHANCED DETECTOR RESOLUTION ALGORITHM ON SPECIFICITY AND SENSITIVITY OF PORTABLE HIGH PURITY GERMANIUM GAMMA DETECTOR SPECTRA

LaTosha M. Bell, BS

June 2009

Approved:

James C. Petrosky, PhD (Chairman)	8Jun09 Date
Larry W. Burggraf, PhD (Member)	8 Jun 2009 Date
Capt Benjamin Kowash (Member)	8 Jun 2009 Date
LTC John McClory (Member)	8 JUN 09 Date

Abstract

The ability to identify special nuclear material is one of the necessary prevention mechanisms for preventing proliferation of special nuclear materials. Additionally, if a nuclear event were to occur, information about the nuclear material used may be extracted from gamma spectra, provided it is obtained quickly and accurately. This can be made possible with the use of the exceptional resolution of the HPGe detector.

This experiment applied the Advanced Synthetically Enhanced Detector Resolution Algorithm (ASEDRA) to a portable HPGe detector's spectra, to investigate whether improvements in specificity and sensitivity can be obtained. This method has been used to improve performance of NaI(Tl) spectra. In this work, measurements of Cd-109, Co-57, Eu-152, Sb-125, Eu-154, and Eu-155 spectra were used as ground truth gamma emissions. The HPGe spectra were analyzed using ASEDRA and ORTEC's Genie™, a program used by many in the nuclear weapons community for spectroscopy. Genie™ was used as a benchmark for comparison in this experiment. The number of positive and false positive peaks identified by each program was used for comparison, based on ground truth peaks, which are the thirty-one known peaks based on the sources used in the experiment.

The results of this work show that Genie™ always locates more ground truth peaks than ASEDRA and that ASEDRA identifies fewer false positive peaks than Genie™ at all but three of the measurement times. In addition, the performance parameter of Genie™ is higher than ASEDRA at short measurement times, implying that ASEDRA does not provide additional spectral information at shorter measurement times. The

application of ASEDRA to experimental spectra does not provide any improvements in specificity or sensitivity, as compared to Genie™.

Acknowledgements

I would first like to express appreciation to my advisor, Dr. James Petrosky, for his support and guidance throughout my time at AFIT. He has continued to challenge me to reach my potential in becoming a better student, researcher, and person and for that I am truly grateful. I am thankful to my committee members Dr. Larry Burggraf, Capt. Benjamin Kowash, and LTC John McClory for their valuable insight and technical expertise which have truly helped me grow as researcher. I would also like to thank laboratory technician, Mr. Eric Taylor, for his continuous assistance and willingness to provide any help needed to complete my research. Most importantly I express sincere gratitude to my husband for his continued love and support during this endeavor. He has helped me to stay focus and has always given me the confidence I needed to succeed throughout this long process and for that I am forever thankful.

LaTosha M. Bell

Table of Contents

Page

List of Figures

Figure Page

List of Tables

EFFECT OF ADVANCED SYNTHETICALLY ENHANCED DETECTOR RESOLUTION ALGORITHM ON SPECIFICITY AND SENSITIVITY OF PORTABLE HIGH PURITY GERMANIUM GAMMA DETECTOR SPECTRA

I. Introduction

1.1 Motivation

The threat of a nuclear attack on domestic soil is a serious concern of the United States government. Part of this concern is due to the spread of weapons-related information and technology in recent years, which has increased the capability for a terrorist to construct a crude nuclear device. Owing to this, the country must be able to quickly assess the type of weapon used and who employed it if a nuclear event were to happen. In addition, the major challenge involved in a terrorist attempting to build a nuclear weapon is the acquisition of special nuclear materials, which requires our nation to have the ability to accurately trace these materials. This has led to an enhancement in the nation's safeguards to prevent such an event from occurring by allowing sources to be traced, which is a deterrent to states that might provide nuclear materials for such a purpose. For example, the Domestic Nuclear Event Attribution (DNEA) program established a policy agenda in which nuclear forensics and attribution capabilities must be improved to help in determining the state origin of fissile material used in a nuclear attack [1].

The safeguards mission of the International Atomic Energy Agency (IAEA) is to give assurance that no declared nuclear material (U, Pu, Th) is diverted to non-peaceful purposes and that no undeclared nuclear material or activities exist in the United States.

To execute its directive, the IAEA completes independent verification measurements of nuclear material using an assortment of Non-Destructive Assay (NDA) instrumentation in attended or unattended mode. This includes High-Resolution Gamma Spectrometry (HRGS) in addition to Room Temperature Gamma Spectrometry (RTGS) which are also important safeguard verification tools. Additionally, the IAEA is seeking to use all available modern technology to enhance its detection capabilities [2].

Prevention mechanisms, such as identification of sources prior to an event taking place, support the primary goal, but there has to be as much effort put into the response following the occurrence of such an event. The Pentagon has created a nuclear forensics team tasked with identifying the attackers should a nuclear weapon be detonated in the United States. The adaptation of nuclear technology to the forensics of an exploded nuclear weapon is an established but developing field [3]. In the event of a nuclear attack, the government will be forced to recover from the attack, while also taking measures to prevent a second attack from occurring. This is extremely vital because, although the effects of a nuclear detonation will be detrimental to the country, the worst thing that could happen after one nuclear attack would be another [4].

1.2 Background

The fallout from a nuclear weapon can be very useful in providing information about the characteristics of the weapon. This essential information can help answer the questions about the type of weapon used and who exploded it. The gamma spectra of the fallout can be measured by using a portable high purity germanium (HPGe) detector. These detectors are commonly used to detect x-ray and gamma radiation as a result of

their unparalleled resolving power and high photon detection efficiency. High resolution is favorable in this application because it can allow for distinction between peaks that are close together, and the high efficiency means short measurement times can be used [5].

Although HPGe detectors have much better resolution than other detectors, such as the NaI(Tl) detector, they still cannot entirely identify every peak present. This can become problematic when attempting to resolve peaks from fallout. Due to the numerous nuclides in nuclear fallout, the peaks in the spectra collected are so close together that discernment of every gamma-emitting isotope present is nearly impossible. The application of the Advanced Synthetically Enhanced Detector Resolution Algorithm (ASEDRA) [6] may be able to improve the specificity and sensitivity of gamma spectra from a HPGe detector. This may allow discrimination of fallout peaks that are close together. This is essential to nuclear forensics because resolving the fission fragment peaks allows the identification of the nuclides present; giving insight to what kind of special nuclear material was used to create the weapon. This information can then be applied to determine who detonated the weapon. ASEDRA may also be able to decrease the amount of measurement time needed. This improvement is vital to the nuclear forensics surrounding the detonation of a nuclear weapon because the time needed to get a useful measurement would be reduced. This would allow a quicker assessment of situation at hand, as well as a reduction in the time that personnel and equipment would have to be exposed to radiation in order to get a measurement that contains enough spectral information.

In previous work where ASEDRA was applied to NaI(Tl) spectra, the improvements seen in the ability to identify more peaks were referred to as improvements in the detector's resolution. The detector's resolution is defined as the FWHM divided by the location of the peak centroid and is intrinsic to the detector material. Therefore, the detector's resolution cannot be improved by the application of a post processing algorithm. Based on this fact, this research will refer to improvements in identifying more peaks as improvements in specificity and sensitivity. Specificity is defined as the true negative fraction which gives the fraction of peaks that are not identified which should appear in the spectrum based on the ground truth. Sensitivity is defined as the fraction of true positive fraction which gives the fraction of peaks that are identified in the spectrum which are ground truth peaks. These parameters are chosen to be used in this research because it encompasses the ability for either program to identify true positive peaks while not identifying false positive peaks which is the essence of what this research is investigating.

1.3 Hypothesis

ASEDRA has been applied to NaI(Tl) detector gamma spectroscopy and provided significant improvement to the specificity and sensitivity of the spectra collected by that detector [6]. Therefore, ASEDRA may be able to improve the specificity and sensitivity of spectra collected by the HPGe detector. This may be applied to the work of nuclear forensics in better identifying fission product gamma peaks in a crowded spectrum as well as decreasing measurement time.

1.4 Research Objectives

1. Develop detector response functions (DRFs) for the HPGe detector using Monte Carlo N–Particle (MCNP) code.

2. Apply ASEDRA, using DRFs, and also the gamma spectroscopy and analysis software Genie™ to measured spectra.

3. Analyze spectra to determine if specificity and sensitivity has improved based on using ASEDRA versus the Genie™ software.

1.5 Scope

This research aims to examine if the application of ASEDRA to spectra collected with the HPGe detector leads to improvements of the specificity and sensitivity compared to that of the gamma spectroscopy acquisition and analysis software Genie™. Both programs are used to analyze HPGe spectra from ten separate measurements, each taken for nineteen different time intervals. Genie™ and ASEDRA both strip the background from the spectra prior to analysis. The comparison between the two programs is based on the ground truth, which are the thirty-one peaks that are known based on the sources used in the experiment. This is done by using the ground truth to compare the number of positive peaks versus false positive peaks located by each program. This process will be explained in greater detail in the following chapters. This research only compares ASEDRA to Genie™ and not any other gamma spectroscopy acquisition programs. In addition, this experiment only examines whether a peak was or was not located and not the uncertainty in locating that peak.

1.6 Approach

MCNP will be used to model the experimental setup in order to create the DRFs that will be used in ASEDRA. The DRFs will be created for energies of 20 keV, 50 keV,

100 keV, and every 50 keV thereafter up through 3000 keV. The experiment will be conducted with a source-to-detector distance of 0.50 m and the sources being used have gamma energies that range from 45-1597 keV. There will be ten measurements taken in this configuration with each of the ten measurements consisting of nineteen different measurement times ranging from 1 to 70560 sec. Once all ten measurements are completed, the resulting spectra will be imported into both Genie™ and ASEDRA for analysis to determine the number of positive and false positive peaks identified for each measurement.

1.7 Paper Organization

This thesis consists of five chapters. The first chapter is an introduction to the thesis and explains the motivation for the research. It also gives an overview of the problem being examined and the steps that were taken to investigate the issue at hand. The second chapter discusses the theory of this research effort with detailed information about the detector and analysis programs used in this thesis. The third chapter gives a detailed look at the methodology used in this research. It includes the specifics of the MCNP generated DRFs in addition to experimental procedures. The fourth chapter explains the results and analysis of the comparison of Genie™ and ASEDRA. This chapter compares the application of Genie™ and ASEDRA to correctly locate peaks. The fifth and final chapter contains the conclusions as well as recommendations for future work in this area

II. Theory

2.1 Gamma Spectroscopy

Gamma-ray spectroscopy measures the energy and number of photons emitted by a radioactive source. This is done by the gamma-ray experiencing an interaction that transmits some or all of its energy to an electron in the detector material. The three interactions that play a major role in gamma-ray spectroscopy are photoelectric absorption, Compton scattering, and pair production. The photoelectric absorption process dominates at gamma-ray energies up to several hundred keV. The pair production process dominates at gamma-ray energies above 5-10 MeV. The Compton scattering process dominates in the range between the photoelectric absorption and pair production processes. Figure 1 illustrates the relationship of the three interactions as functions of the absorber material's atomic number and the energy of the incident photon. The most favorable interaction for gamma spectroscopy is photoelectric absorption because the total electron kinetic energy equals the energy of the incident gamma-ray [7].

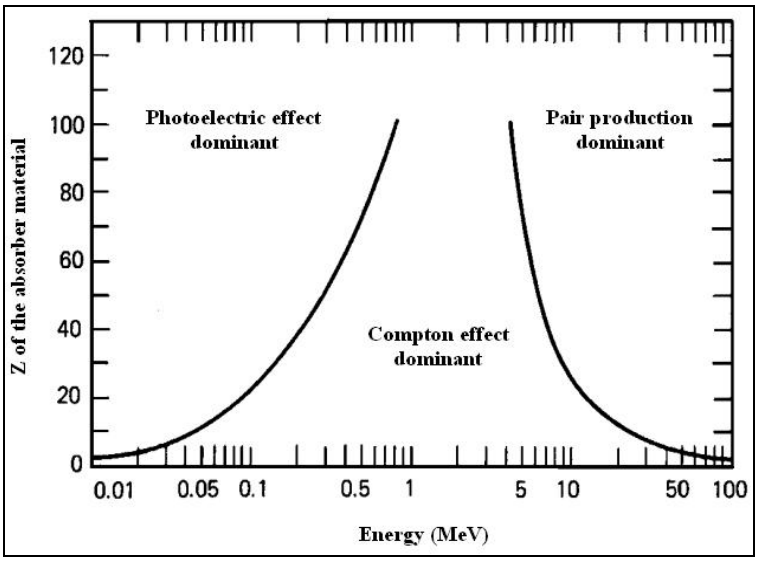

Figure 1. Dominant Regions for Gamma-Ray Interactions [7].

Gamma-rays can Compton scatter with an electron in the detector, and the scattering angle between the incident and scattered gamma-rays determines the energy deposited into the detector. This relationship is shown by Equation (1) where E_c is the energy of the Compton scattered gamma-ray, θ is the scattering angle and $\alpha = E/E_o$ in which E is the incident gamma-ray energy and E_o is 511 keV [7].

$$E_C = \frac{E}{1+\alpha(1-\cos\theta)} \tag{1}$$

Based on the geometry of the source and detector, there are preferred scattering angles which produce counts in the spectra at energies less than the full energy peak (FEP). For small scattering angles there is very little energy transferred, and some of the original energy is always retained by the incident photon, regardless of the scattering angle. This is illustrated in Figure 2 where '1' denotes the FEP, '2' denotes the Compton continuum, and '3' denotes the region of multiple scatters [7].

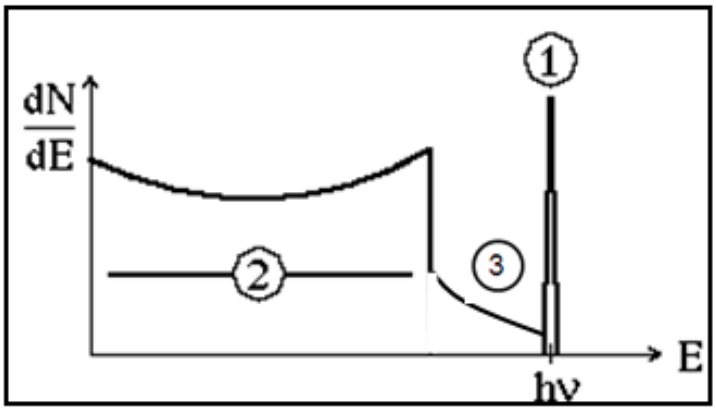

Figure 2. Sample Spectrum Highlighting Full Energy Peak and Compton Continuum [7].

2.1.1 The Effects of Ground Scattering

Ground scattering occurs when the incident photon interacts with the ground or a surrounding material before entering the detector. This causes some of the photon's energy to be transferred to that material leaving the photon with less energy when it enters the detector. This can lead to fewer counts in the FEP and more counts in the Compton region of the spectrum. The effects of ground scattering have to be addressed in this experiment, because ground scattering causes the response of the detector to change. Majer et al. [8] studied the effects of the near-source Compton scattering using a collimator in front of a planar germanium detector to decrease the near-detector scattering. Their investigation of effects of near-source scattering in photon spectra measured with a HPGe detector has demonstrated that a continuous distribution below the full-energy peak, the shoulder, being the region of multiple scatter, previously denoted as '3' in Figure 2, is due to Compton scattering with electrons in non-radioactive source material surrounding the detector sensitive volume. The total numbers of pulses

in the region of the shoulder are approximately proportional to the linear dimensions of the volume and electron density of the scatterer. The shape of the shoulder depends on the distribution of scattering centers relative to the source and detector [8].

Majer et al. [9] continued the study of HPGe detector response functions with improvements to their previous work. The calculations of the shoulder spectra were improved by considering broadening due to electron momentum distributions in Compton scattering and double Compton scattering. The only modifications made in measurements with each of the gamma-ray sources described in this follow-up work were different orientations of the source plates. The very dissimilar shoulder spectra indicate that they are generally due to the near-source scattering, in spite of the small masses of the source plates. Reorientations of the sources produce different distributions of angles of Compton scattering and different energy distributions of secondary Compton photons that penetrate the detector. In this measurement better fits were attained than with the previously reported spectra. The shoulders in the newly measured spectra are also well explained with the calculated ratios of the numbers of counts in the shoulders and in the corresponding full-energy peaks being in reasonable agreement with the experimental ratios.

Uroic et al. [10] set out to reduce the source of scattered radiation into the detector sensitive volume with the goal of improving the measured spectra. To lessen the near-source scattering, a very small source of ^{241}Am was prepared along with a shield and two collimators. There were three principal scattering materials considered in the calculations of the scattering effects: near-source scattering in Am and neoprene glue, small-angle

scattering from the collimator edges and lead shield, and large-angle backscattering from the copper plate located on the inside of the lead shield. Owing to the reduction of the single-scattering processes, the multiple-to-single-scattering ratio was also reduced. Therefore, the double and multiple scattering events were negligible and as a result only the single Compton scattering was calculated. The measurements indicate that in the 25–100 keV energy range, the quality of the photon spectra measured with HPGe detectors can be significantly improved if near source scattering effects are greatly reduced. The use of an extremely small source and collimation has improved the shoulder-to-FEP ratio by as much as a factor of 10. In addition, the principal cause of non-FEP events is the near-source scattering. This implies that in the energy range measured, modeling of the line profile should be source and shield dependent, rather than detector dependent.

Plagnard et al. [11] studied photon-scattering effects in the 15–80 keV low-energy range with planar and coaxial HPGe detectors. In the low-energy range, spectra shapes are strongly disturbed by parasitic bumps due to scattered events. These effects are mainly important in the energy range lower than 60 keV where the FEP and the bump overlap. This experiment examined the influence of the environment close to the source in the 20–30 keV energy range. This effect can be decreased by carefully selecting the geometry and material of the source holder. Furthermore, the implementation of an adapted geometry with collimators ideally distributed between the source and the detector allows for a reduction in scattering. However, because the scattering sites depend on energy, it can be difficult to define an optimum geometry for the whole energy range of interest.

The four experiments described in the previous section demonstrate the significant effect that scattering has on the measured spectra, particularly in the lower energy range. These results confirm the necessity of considering the effects of ground scatter in the detector response functions.

2.2 HPGe Detector

Though solid state devices offer many advantages to radiation detection, their performance is limited by the achievable depletion depth. Silicon or germanium p-n detectors of normal semiconductor purity cannot achieve depletion depths beyond 2-3 mm. In order to perform gamma-ray spectroscopy, the thickness of the depletion region must be larger. The thickness of the depletion region is given by Equation (2)

$$d = \left(\frac{2\varepsilon V}{eN} \right)^{\frac{1}{2}} \tag{2}$$

where V is the reverse bias voltage, N is the net impurity concentration in the semiconductor, ε is the dielectric constant and e is the electronic charge. At a specific voltage, the impurity concentration is the only parameter that can be changed to achieve a greater depletion region. This is accomplished by implementing refining techniques that reduce the impurity concentration to approximately 10^{10} atoms/cm^3. With this impurity level, a depletion depth of 10 mm can be obtained for voltages less than 1000 V [7].

The HPGe detector is preferred for the identification of special nuclear material because of its resolution compared to other types of detectors. Figure 3 depicts the difference in resolution in several gamma-ray detectors.

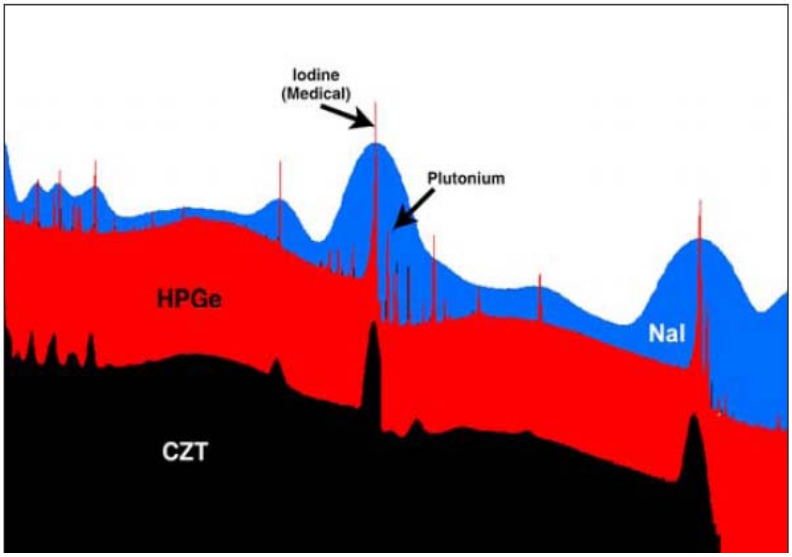

Figure 3. Gamma-Ray Spectra of Natural Background Using Various Detectors [12].

This section demonstrates the advantages of HPGe detectors compared to other gamma-ray detectors. For the application of identifying special nuclear material, HPGe detectors are of particular interest because of their outstanding resolution.

2.3 MCNP

MCNP is a general purpose Monte Carlo code that can be used for neutron, photon, and electron transport. This code treats an arbitrary three-dimensional configuration of a material in geometric cells bounded by first- and second-degree surfaces and fourth-degree elliptical tori. The code accounts for incoherent and coherent scattering, the possibility of fluorescent emission after photoelectric absorption, and absorption in electron-positron pair production for photons. MCNP generates results by simulating single particles and recording some characteristics of their average behavior. The common behavior of particles in the physical system is then concluded from the

average behavior of the simulated particles. This is done by using the central limit theorem, which states that the sampling distribution of a sample's mean approaches that of a normal distribution with a mean the same as the population and a standard deviation equal to the standard deviation of the population divided by the square root of the sample size, with increasing sample size [13].

In particle transport, the Monte Carlo technique is a method of simulation used often. It consists of actually following the particles from a source, throughout their life to their death. Probability distributions are randomly sampled using transport data to determine the outcome at each step of the particle's life. Figure 4 illustrates the random history of a neutron incident on a slab of fissionable material.

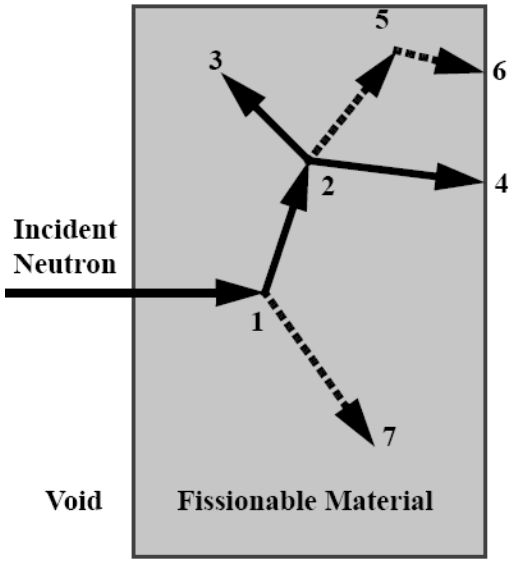

Figure 4. Random History of Neutron in MCNP [13].

In this particular example, a neutron collision occurs at event 1. The neutron is scattered in the randomly selected direction illustrated. A photon (particle 7) is also

produced and temporarily stored for later analysis. At event 2, fission occurs, resulting in the termination of the incoming neutron and the birth of two outgoing neutrons and one photon. One neutron and the photon are banked for later analysis. The first fission neutron is captured at event 3 and terminated. The banked neutron is now retrieved and, by random sampling, leaks out of the slab at event 4. The fission-produced photon has a collision at event 5 and leaks out at event 6. The remaining photon generated at event 1 is now followed with a capture at event 7 [13].

2.3.1 The Use of MCNP

The use of Monte Carlo codes has become essential to the study of radiation detectors. Owing to this, efficient and accurate Monte Carlo codes need to be available for use. Vidmar et al. [14] performed a study of the most commonly used Monte Carlo codes in gamma-ray spectrometry. This was done in order to determine how much the results of different codes differ from one another when full-energy-peak and total efficiencies are computed for well-defined sample-detector arrangements. While it was possible to obtain uniform results from different users of the same code and to a large extent from different versions of the same code, the disparities between the codes turned out to be astoundingly large, reaching 10% in some cases at lower energies. The reasons for those discrepancies continue to be investigated. More favorable results can be anticipated at higher energies, above 200 keV, and when the codes are used in the (relative) efficiency-transfer mode in particular, with the differences reduced to 1%. The statistical uncertainties of the calculated efficiencies were kept at 0.3%. Although there were some differences between the Monte Carlo codes investigated, none of the codes

tested, including Monte Carlo N–Particle (MCNP), was deemed to be unacceptable for gamma-ray detection modeling.

With increased computational power, Monte Carlo simulations of detector systems have become a complement to experimental detector work. Determining sample self-absorption corrections or simulating entire in-situ gamma-ray spectrometry measurements are two such applications. Nonetheless, when calculating the detector response for HPGe detectors through Monte Carlo simulations, one often observes a discrepancy between calculated and empirical data. Monte Carlo calculated efficiencies are typically 10–20% higher than what is found experimentally. This deficiency in the observed detector efficiency is commonly attributed to uncertainties, often an underestimation, in the thickness of the dead layer caused by the n+ contact. Therefore, this thickness is often adjusted in the model to match Monte Carlo calculated efficiencies with experimental ones [14].

In the work of Boson et al. [15], there were some discrepancies found in some of the initial Monte Carlo simulations of the HPGe detector. The purpose of the Boson et al. [15] work was to meticulously study the response of the HPGe detector and to deduce the cause of any eventual efficiency deficit found. They constructed a model using the MCNP5 code which was used to simulate the empirical efficiency calibrations. The full-energy peak efficiency was determined using the pulse height tally for the same set of photon energies and angles of incidence that was used for the empirical calibration. There were a sufficient number of Monte Carlo histories run to ensure a variance in the estimate below 3%. This experiment resulted in a lower efficiency of the real detector

compared to the MCNP model. It was determined that this is most likely due to a dead layer thicker than stated by the manufacturer. The dead layer was estimated to be approximately 1.5 mm, which was about twice the stated value. This results in both a thicker absorbing layer as well as a decreased active crystal volume, and is sufficient to explain the observed decrease in detector efficiency. The Monte Carlo detector model was then adjusted in accordance with results from the dead layer measurements. The correction factors that were derived can be used with MCNP, based on manufacturer supplied data, to accurately reproduce experimental efficiency results [15].

MCNP has also been useful in the comparison of a variety of detectors. In the work of Ayaz-Maierhafer et al. [16], the absolute total efficiency and the absolute peak efficiencies for ^{60}Co, ^{137}Cs and ^{241}Am were simulated and compared for common radiation detection materials. The detectors NaI:Tl, CdZnTe, HPGe, HPXe (High Pressure Xenon), $LaBr_3$:Ce and $LaCl_3$:Ce were compared relative to a 188.82 cm x 60.96 cm x 5.08 cm polyvinyltoluene (PVT) plastic scintillation detector using MCNP. The absolute peak detection efficiencies of some detectors were higher relative to PVT, including the absolute peak detection efficiency of NaI:Tl, HPGe , HPXe , and $LaCl_3$:Ce for all geometries studied. These results show that the gamma-ray spectroscopic limitation of PVT in portal monitors can be overcome by using other common detector materials, like HPGe.

MCNP is also being used to predict the response of HPGe detectors in a large assortment of detector-source geometries. The accurate simulation of germanium detectors in response to incident gamma rays relies on an understanding of the

performance of the detector in various detector-source geometries. In the work of Keyser et al. [17], the efficiency as a function of incident pencil beam gamma rays was measured for HPGe detectors of various crystal types at different energies. The experimental data demonstrated that individual detectors can have different sensitivities along the length of the crystal. These detailed measurements were used to characterize the detector for the MCNP calculations, in which the result for the peak sensitivities was shown to duplicate some of the individual detector differences. The detector construction and crystal particulars are essential before correct MCNP calculations can be completed, although this, by itself, is not adequate to reproduce the detector response for all environments.

In-situ gamma-ray spectrometry is increasingly used in many applications, such as geophysical exploration, assessment of doses to the population due to radioactive fallout, and determination of soil erosion rates employing the ^{137}Cs technique. Portable gamma spectrometry can be used instead of the conventional method or combined with it, allowing measurements to be performed more rapidly and thereby wider areas to be surveyed. The main shortcoming of in-situ spectrometry for soil erosion measurements is that because the radionuclide depth distribution in the soil is unknown, the calculated ^{137}Cs inventories are uncertain. A solution proposed to overcome this drawback consists in considering not only the 661.7 keV photopeak count rate but also the peak-to-forward scatter ratio. In the work of Gutierrez-Villanueva et al. [18], MCNP is used to approximate ^{137}Cs inventories. The results of their work demonstrate that Monte Carlo simulations applied to ^{137}Cs inventory measurements by field gamma-ray spectrometry are an important tool which permits the number of experimental measurements necessary

to calibrate the method to be reduced. The MCNP code has been confirmed to correctly duplicate efficiency values and peak-to-forward scatter ratios for a portable HPGe detector. In addition, the use of Monte Carlo methods allows replicating any density and soil chemical composition, thereby improving the accuracy of the results.

In the work described in this section, the use of MCNP has been shown to accurately simulate the response of the HPGe detector in certain controlled situations. This section has also described the various applications in which MCNP can be used and how MCNP simulations can become a compliment to some experiments.

2.4 ASEDRA

ASEDRA is used to post-process detector spectra to better "resolve" photopeaks with high accuracy. The first and critical step in processing a gamma spectrum begins with a robust noise removal process. This is particularly important for spectra with few counts because it allows for true features of the spectrum to more easily seen. The Adaptive Chi-square Processed (ACHIP) algorithm [6] is used to remove noise from the spectra without removing the important details. This Chi-square analysis establishes whether a difference between counts in adjacent channels, understood to have comparable uncertainties, is statistically significant, or if it is truly noise. The criteria of whether or not the data is "noise" is based on three criteria: (1) a user-specified significance value, alpha, (2) the number of collected points measured, and (3) the associated confidence interval allocated to the significance value for the data. The Chi-square metric computed for actual values n_i vs. "expected" modeled values $E(n_i)$ in adjacent channels is shown in Equation (3) [6].

$$X^2 = \sum_i \frac{\left(n_i - E(n_i)\right)^2}{E(n_i)} \tag{3}$$

The ACHIP tool uses a Chi-square basis with the given alpha value for stochastic noise removal at each data point in a spectrum by parabolic fits. It begins with three channels, the center one being the channel of interest, where noise is to be removed. The parabolic model is initially fit to the original three points by means of a least squares fit. Additional neighboring points are considered, with the data point of interest in the center, where new parabolic fits for all points are determined. Once the parabolic model for the data points considered no longer meets the user-specified Chi-square test metric, the model that just previously satisfied the Chi-Square criteria, using n-1 points fit, is used. In Figure 5, the left plot is a Monte Carlo pulse height tally and the right plot is the same tally with noise removal by ACHIP. It is important to note that the significant details of the spectrum are preserved, and stochastic artifacts are nearly all removed [6].

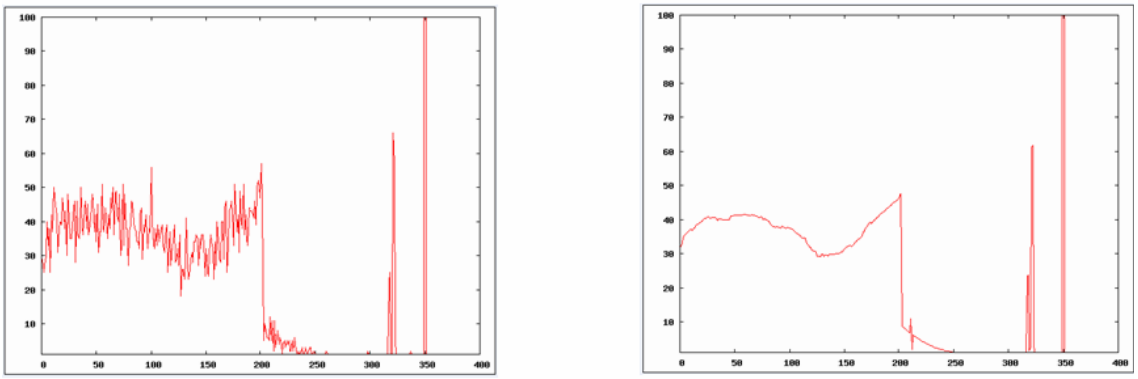

Figure 5. Spectrum Before and After Application of ACHIP [6].

In order to use ASEDRA, detector response functions generated by MCNP, have to be applied. Then the response functions must be broadened to represent responses in real detector systems. This is accomplished by applying a Gaussian function with a detector and energy dependent, low energy tailing correction. This is based on a simple energy-dependent Full-Width-at-Half -Maximum (FWHM) table and energy calibration file spanning the energies of interest, which are treated by ASEDRA as piecewise linear functions. ASEDRA begins searching for peaks at the high-energy end of the detector recorded spectrum, and finds one photopeak at a time. It then subtracts the entire detector response for that photopeak, as determined by the MCNP generated response function. This process continues until no further photopeaks can be identified. A flow diagram of how ASEDRA processes spectra is shown in Figure 6 [6].

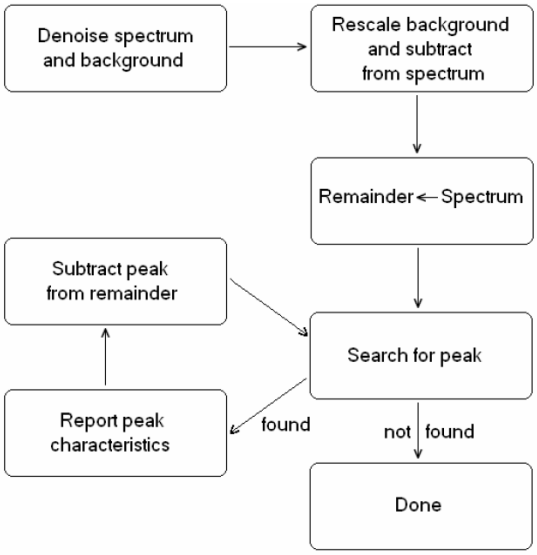

Figure 6. Flowchart of ASEDRA Processing Spectra [6].

2.4.1 The Application of ASEDRA

ASEDRA is used to improve the specificity and sensitivity of measured spectra. LaVigne et al. [6] performed an experiment using a 10 minute measurement of shielded Weapons Grade Plutonium (WGPu) with a NaI(Tl) detector. A considerable number of WGPu peaks were extracted by ASEDRA and are shown of the left side of Figure 7. These peaks were validated by a co-located, calibrated HPGe detector, whose spectrum is shown on the right side of Figure 7.

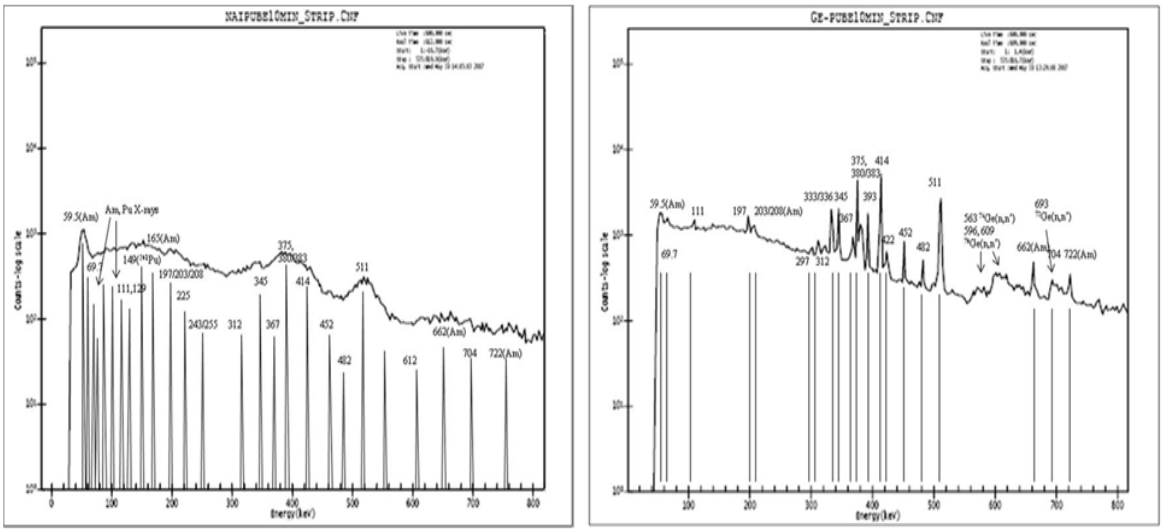

Figure 7. ASEDRA Processed NaI(Tl) Spectrum (Left) Identifies 90% of WGPu Gamma Peaks That HPGe Detector Spectrum (Right) Identifies Using Same Source and Geometry [6].

Initial results illustrate that ASEDRA directly identified numerous Pu gamma peaks, which correlated extremely well to HPGe results, as designated by the labeled gamma lines. Preliminary analysis of the results revealed ASEDRA correctly identified over 90% of the gamma peaks, even those in the low energy region that are too

complicated to identify using HPGe due to the inherent Compton scattering in similar regions of the HPGe detector spectrum [6].

Detwiler et al. [19] extended the work of LaVigne et al. [6] by improving the shielded Pu identification with the application of ASEDRA. In this experiment, spectra of a WGPu source enclosed in a cylindrical composite metal shield were taken with NaI(Tl) and HPGe detectors. The ASEDRA peaks and key lines from the HPGe spectra are shown in Figure 8 [19].

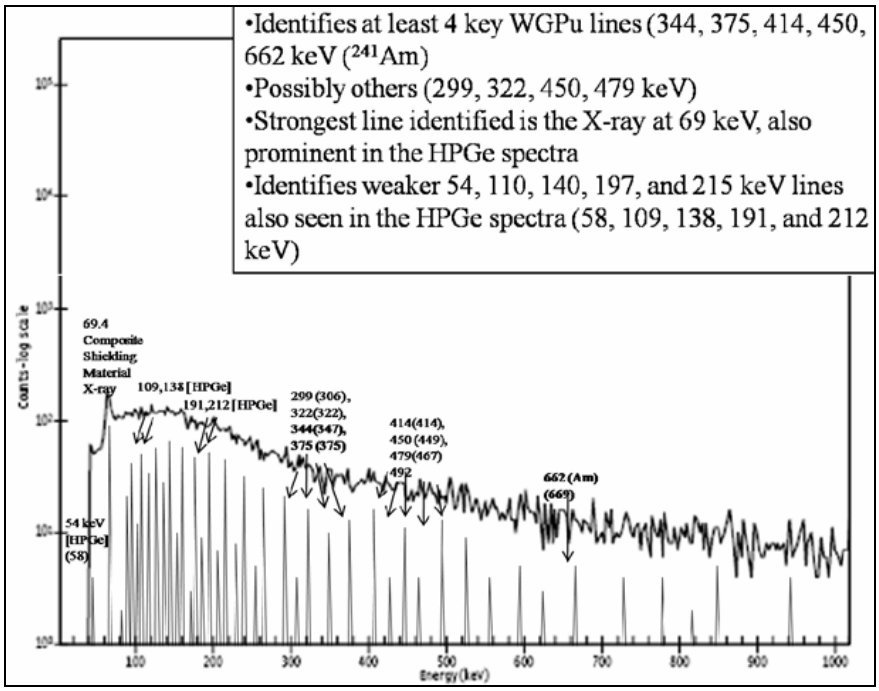

Figure 8. ASEDRA being Applied to NaI(Tl) WGPu Spectra [19].

The NaI(Tl) spectra processed by ASEDRA provided results for WGPu energies identified to within 1 % and one-half of a FWHM with standard settings and calibration. The ASEDRA smoothing and fitting of NaI(Tl) spectra generates results similar to that of a higher resolution detector, with no previous information on the spectra. For side-by-side

comparisons, the ASEDRA-processed NaI(Tl) results found virtually all of the photopeaks found by the HPGe detector, not including several weaker peaks narrowly spaced in energy from a more predominant peak. Nevertheless, some weaker lines were identified by NaI(Tl)-ASEDRA and not located by the HPGe detector. The accuracies of photopeak energies are comparable to those from a detector of 1% resolution for runs with good statistics [19].

This section shows how the application of ASEDRA improves the specificity and sensitivity to of the NaI(Tl) collected spectra to equal or even better than that of spectra taken with a HPGe. This work shows that the application of ASEDRA can improve specificity and sensitivity for NaI(Tl) detectors, and the hope is to also improve the same using HPGe detectors.

2.5 Genie™

Genie™ [20] is a gamma spectroscopy software package with the capability of acquiring and analyzing spectra. In this experiment, a spectral file is imported into Genie™, a calibration file is loaded into it, and a peak search routine is applied to the spectrum.

The calibration file that is loaded into the spectrum is created within Genie™. The calibration file used in this research effort was produced using an energy-only calibration. This method allows the calibration to be completed by using energy/channel pairs by either the Cursor or Manual Method. For the Cursor Method, a spectrum must be in the spectral display area and its cursor must be on the peak that is being used for calibration. The Cursor button is then selected in order to add that particular channel position to the

Channel text box. Finally the known energy value must be entered into the Energy text box to add that data point to the calibration. For the Manual Method, the spectrum does not have to be displayed in the spectral display area. To add an entry to the calibration file, an energy value for the peak being used must be entered into the Energy text box and the corresponding channel number in the Channel text box. This process is completed for all of the peaks used in the calibration [20].

Genie™ has five algorithms for locating peaks in a spectrum. For this particular research the VMS Standard Peak Search was used. This method performs a second difference peak locate followed by a pure Gaussian fit peak analysis. The dependable determination of the background under a photopeak is very important to this peak search algorithm. The main contributions to the background are the ambient and the Compton backgrounds. A third background component is called the "step background" and is based on the assumption that a gamma-ray can undergo more than one interaction. This then causes multiple Compton events that have the ability to contribute to channels just below the photopeak. This "step background" is solved using an analytical formula.

Once the background is accounted for, the algorithm calculates the gross counts in the peak region, as the sum of the individual channel contents over the entire peak region. The contribution to the peak area for each channel is then solved for simply using the gross counts in that channel less the background contribution for that channel. The peak area is determined to be the sum of the contribution to the peak area for each channel, or just the gross counts less the background. From the previous values calculated, the uncertainty in the peak area can then be solved. Lastly, the peak centroid channel is

determined by using a first moments calculation which includes the contribution to the peak area for each channel, the peak area, and the channel that defines the left limit of the peak region [21].

III. Methodology

3.1 Determination of Measurement Site

This research began with the determination of the measurement site in which the least amount of background noise existed. This was done in order to ensure that the background radiation of the experimental environment contributed as little as possible to the experimental measurements. This was accomplished by using the HPGe detector to take overnight background measurements in several labs in Bldg 470 at Wright-Patterson AFB. The spectra taken in each site were compared to determine which location provided the smallest amount of background radiation. The shape of all three spectra were similar and Table 1 shows the counts per second (CPS), over the entire spectrum, at each of the three locations examined. This preliminary analysis determined the secure computing room to be the optimal location for measurements in this experiment.

Table 1. Background Measurements of Potential Experimental Locations

Location	CPS
Lab 107	47.96
Basement	44.72
Secure Computing Room	38.69

3.2 Calibration of HPGe Detector

The detector used in this experiment was the Ortec® Detective-EX-S portable HPGe detector. It is a coaxial p-type detector with a 50 mm diameter and 30 mm deep Ge crystal and low power Stirling Cooler. The detector is shown in Figure 9.

Figure 9. Ortec® Detective EX-S portable HPGe Detector

A calibration of the HPGe detector was performed using a multi-nuclide source and the gamma-ray spectroscopy software GammaVision®. The calibration was taken in the secure computing room with the source at a distance of 15 cm from the front face of the detector, on axis with the crystal. The measurement of the multi-nuclide source was taken for 24 hours to make certain that ten peaks would be located in the calibration spectrum. The 10 peaks from the multi-nuclide source used in this energy calibration are shown in

Table 2 [22]. The certificate of calibration for the multi-nuclide source is given in Appendix A.

Table 2. Calibration Gamma-Ray Peaks [22].

Nuclide	Energy (keV)
Am-241	59.54
Cd-109	88.03
Co-57	122.06
Ce-139	165.85

Sn-113	391.70
Cs-137	661.66
Y-88	898.04
Co-60	1173.24
Co-60	1332.50
Y-88	1836.06

The gamma energies from various sources used in this thesis are within 1 keV of one another, which means the detector calibration should be better than that. To test the validity of this calibration, measurements were taken with a Eu-152 and a Na-22 source, with the gamma-ray energies from each nuclide shown in Table 3 [22]. The certificate of calibration for the Eu-152 and Na-22 sources are given in Appendices B and C.

Table 3. Calibration Verification Gamma-Ray Peaks [22].

Nuclide	Energy (keV)
Eu-152	121.78
Eu-152	344.28
Na-22	511.00
Na-22	1274.53
Eu-152	1408.01

It was determined that these measured gamma energies ranged within 0.13-1.59 keV of their known values. This error is too large for this research, so either the calibration equation has to be adjusted or more points have to be used for the calibration. Because adding more sources to the calibration meant that there would be fewer sources to validate the calibration, it was decided that the energy calibration equation needed

some modifications. There was an attempt to adjust the energy calibration equation in GammaVision®, but the software did not allow for changes to the energy calibration equation. The ten point calibration that was generated using GammaVision® was therefore completed using Genie™, a gamma spectroscopy acquisition and analysis software program. The Genie™ software allowed for the coefficients in the energy calibration equation to be slightly adjusted for a best fit to the 10 calibration peaks. This was done in order to allow for the measured gamma energies, from the Eu-152 and Na-22 sources, to range from 0.16-0.26 keV of their known values and the ten gamma energies from the calibration source to vary from 0.11-0.38 keV of their known values. The equation for the energy calibration is shown in Equation (4) and plotted in Figure 10.

$$EnergyCalibration = 0.1502\ \text{keV} + 0.3656 \times \text{Channel} \quad (4)$$

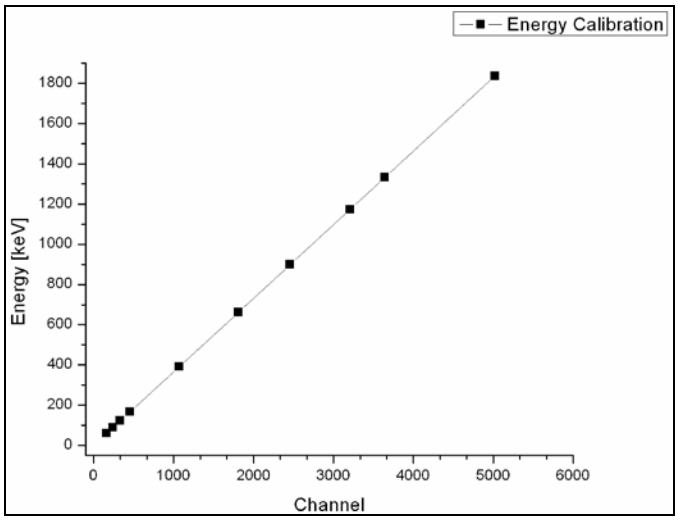

Figure 10. Genie™ Energy Calibration

To make certain that the detector calibration was not affected by any environmental conditions, 24 hour measurements, were taken using the detector's Cs-137 test source. Following each measurement, the spectrum was analyzed using the Genie™ software to determine the energy location of the 662 keV peak centroid. This energy is plotted in Figure 11 for each day a measurement was taken to observe if the calibration changed over time.

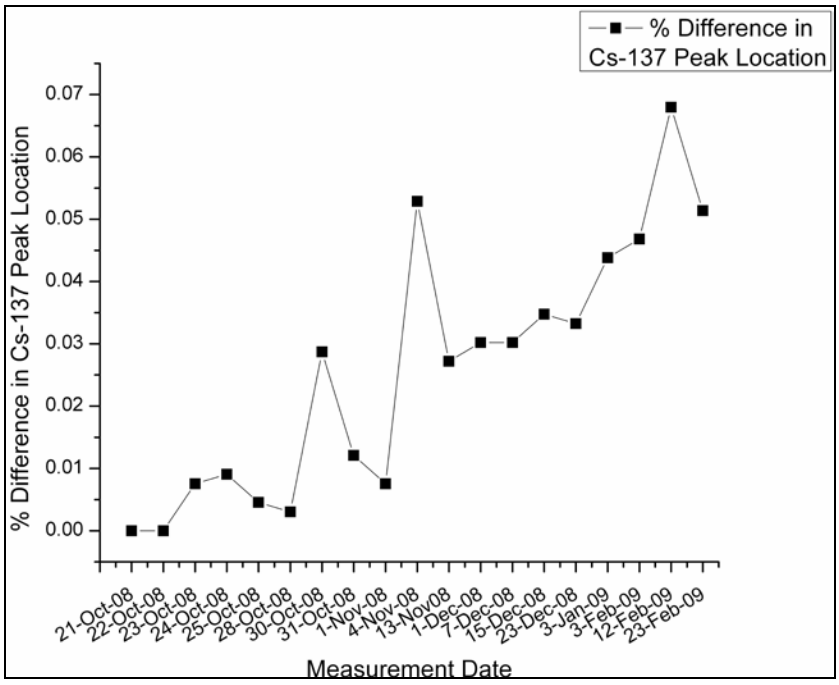

Figure 11. Percent Changes in 662 keV Peak Locations.

As displayed in Figure 11 the location of the 662 keV peak does drift during the duration of the experiment, but it does not vary by more than 0.07%. This confirms that the calibration used throughout the experiment was valid to within that amount. Throughout the experiment, background measurements were taken to ensure the

environment of the measurement site stayed consistent for the duration of the experiment. The background measurements are plotted in Figure 12.

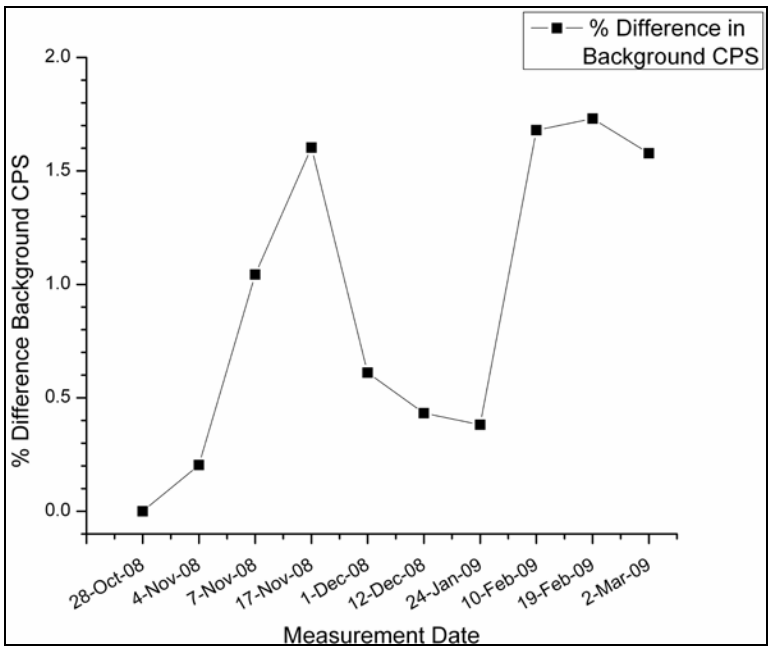

Figure 12. Percent Changes in Background CPS.

Figure 12 illustrates that the maximum change in the background of the room used during this experiment was only 1.7%. This minute variation in the background verifies that the environment in which these measurements were performed did not have a notable effect on the experimental results.

3.3 MCNP Generated Detector Response Functions

Once the calibration was complete, measurements were taken in the secure computing room with the multi-nuclide source at various distances. This was done prior to the main experiment to compare the experimental spectra to those produced by MCNP and to verify that the two methods, experimental and modeling, matched sufficiently. It

was also done to investigate if the detector-to-source distances had an effect on the relationship between the experimental and MCNP generated spectra. There were 6 measurements taken at distances of 15, 35, 50, 65, 80, and 100 cm for counting times of 10, 20, 30, 40, 50, and 60 minutes correspondingly. The same set of measurements was taken with a Cs-137 source to also compare with the MCNP spectra. It was determined that there was no significant variation in the spectra among the various distances examined, so the 50 cm distance was chosen to be used in the main experiment.

In the MCNP simulations, the modeling of the HPGe detector used was previously completed by MAJ Randall Rockrohr in his work with determining source position of SNM using the HPGe detector. The source used in the MCNP simulations was modeled as a point source. To ensure that the experimental source could be modeled as a point source, the effective solid angle of the detector for a point source and circular disk source at a distance of 50 cm was calculated. This was done to prove that at this distance, the experimental source being modeled as a point source is valid by showing that the effective solid angle of the detector for a point and circular disk source are essentially the same at this distance. The solid angle for a point source is given by Equation (5) [7]

$$\Omega = 2\pi\left(1 - \frac{d}{\sqrt{d^2 + a^2}}\right) \tag{5}$$

where d = 50 cm, the distance between source and detector, a = 2.5 cm, the radius of the detector, and s = 1.5 cm, the radius of the source. The solid angle for a point source was calculated to be 0.007839. The solid angle for a circular disk source is given by Equation (6) [7]

$$\Omega = 2\pi\left[1-\frac{1}{(1+\beta)^{1/2}}-\frac{3}{8}\frac{\alpha\beta}{(1+\beta)^{5/2}}+\alpha^2\left[F1\right]-\alpha^3\left[F2\right]\right] \tag{6}$$

where

$$F1=\frac{5}{16}\frac{\beta}{(1+\beta)^{7/2}}-\frac{35}{64}\frac{\beta^2}{(1+\beta)^{9/2}}, \tag{7}$$

$$F2=\frac{35}{128}\frac{\beta}{(1+\beta)^{9/2}}-\frac{315}{256}\frac{\beta^2}{(1+\beta)^{11/2}}+\frac{1155}{1024}\frac{\beta^3}{(1+\beta)^{13/2}}, \tag{8}$$

$$\alpha=\left(\frac{s}{d}\right)^2, \quad and \quad \beta=\left(\frac{a}{d}\right)^2. \tag{9}$$

The solid angle for a circular disk source was calculated to be 0.007834. The difference in the two calculations was 5.26×10^{-6}, 0.07%. This difference in the solid angle of a point and circular disk source shows that the point source approximation used in MCNP is valid at a distance of 50 cm, which is the distance used in the main experiment.

The MCNP simulations were completed with and without a concrete scattering ground plane to find out which simulation more closely matched with the experimental setup. The spectra from the two simulations were compared to the experimental spectrum by inspection of the spectra as well as applying the Pearson Moment Product Correlation. Pearson's correlation determines the degree of linear relationship between the two spectra, where zero is no correlation and one is perfect positive correlation. This

Pearson Moment Product Correlation analysis determined that the correlation between the scattering plane modeled and experimental spectra was 0.4091 and between the experimental and no scattering plane modeled spectra was 0.3865. The application of the Pearson Moment Product Correlation demonstrates that the MCNP simulations using the concrete scattering ground plane resulted in spectra that correlated better with the experimental spectra than without the scattering ground plane. This comparison is shown in Figure 13 with the spectra normalized to the same number of peak counts.

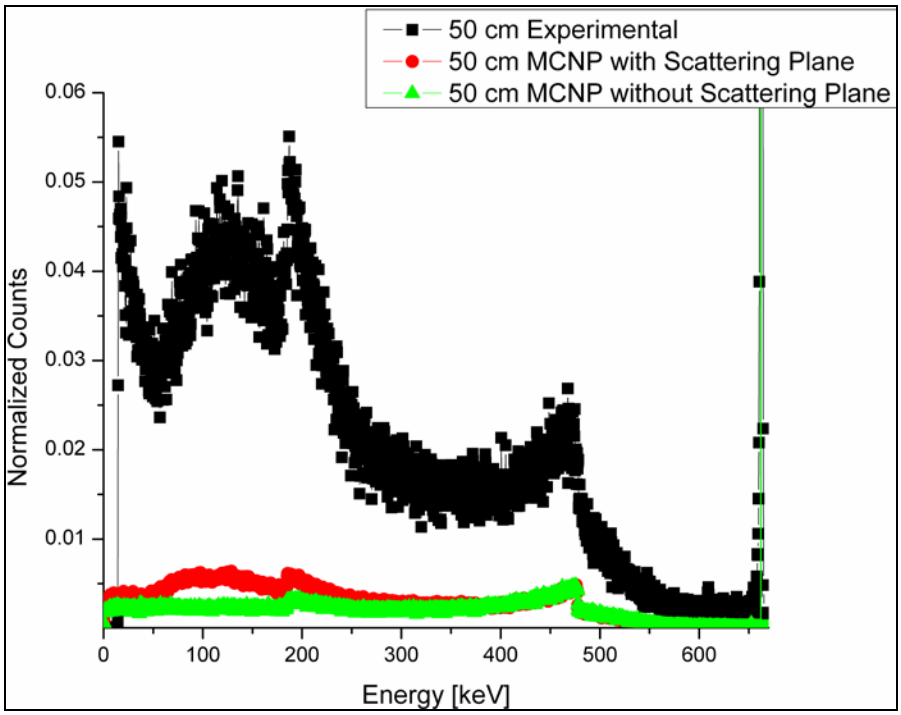

Figure 13. Experimental Spectrum Compared with MCNP Generated Spectra With and Without a Scattering Plane.

The difference in counts between the experimental and MCNP generated spectra can be attributed to various mechanisms. The central reason for the differences is that

MCNP is merely a model. All the characteristics that contribute to an actual HPGe spectrum are not able to be coded in the model, making MCNP not able to completely duplicate the experimental spectrum. It is important to note that although MCNP simulation results in fewer counts in the spectrum than the experimental spectrum, the MCNP generated spectrum has the same shape as the experimental spectrum which is essential for using MCNP to create the DRFs.

All of the previous MCNP runs were completed using the thick-target Bremsstrahlung model (TTB) because of the substantial amount of computational time required using the full physics package. The TTB model produces electrons, but assumes that they are locally slowed to rest. The electrons that are not transported produce Bremsstrahlung photons, which inherit the direction of the parent electron, and are then banked for later transport. Consequently, electron-induced photons are not ignored, but the time expensive electron transport step is omitted [13].

To establish whether the full physics package is necessary in this experiment, an MCNP simulation of the Cs-137 source at 50 cm was completed using the full physics package. This simulation was then compared to that using the TTB model to determine if the information gained was worth the computational time to complete the simulation. The MCNP simulation of the Cs-137 source at 50 cm using the TTB model took 45 minutes, whereas the same simulation using the full physics package took 15 hours. The results of using the full physics package compared with the TTB modeled spectra are shown in Figure 14.

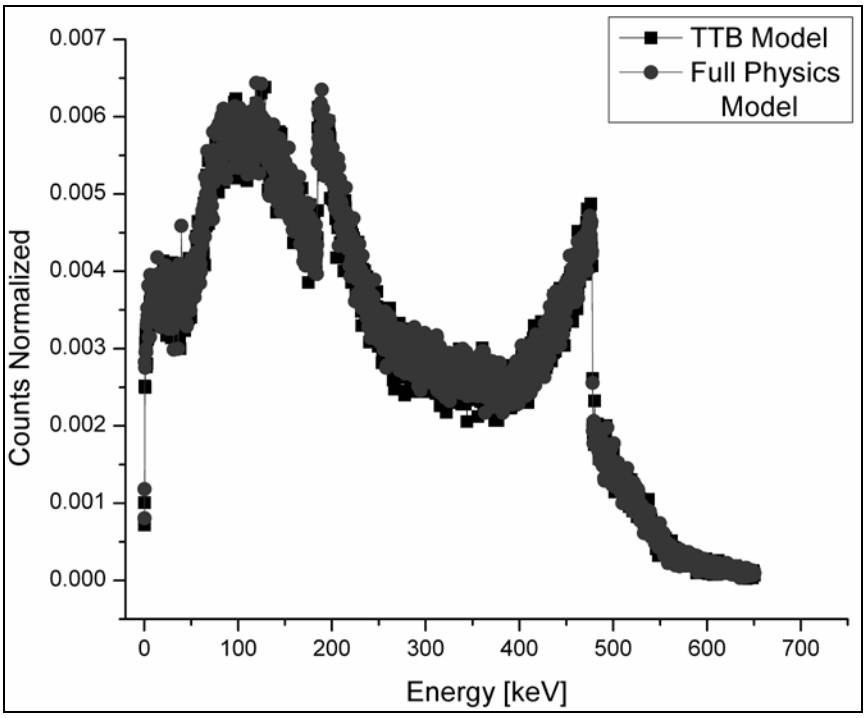

Figure 14. Full Physics Package Spectrum Compared With TTB Modeled Spectrum.

To verify if the TTB modeled spectrum indeed gives the same results as the full physics model spectrum, statistical analysis was completed on both spectra. The Pearson Moment Product Correlation was applied to test the correlation between the TTB and full physics modeled spectra. Pearson's correlation determines the degree of linear relationship between the two spectra, where zero is no correlation and one is perfect positive correlation. This Pearson Moment Product Correlation analysis determined that the correlation between the TTB and full physics modeled spectra was 0.99996, which is practically perfect correlation. In addition to the Pearson Moment Product Correlation analysis, the difference between counts in each energy bin was calculated and is plotted in Figure 15. This illustrates that the difference between the TTB and full physics modeled spectra is miniscule as can be seen by the slight variations above and below

zero. Also, the mean of the differences was calculated to be 0.000775 which further demonstrates that the spectrum using the full physics package closely resembles the results of the TTB model. This led to the decision to only use the TTB model because of the computational time that would be saved, nearly fourteen hours per simulation.

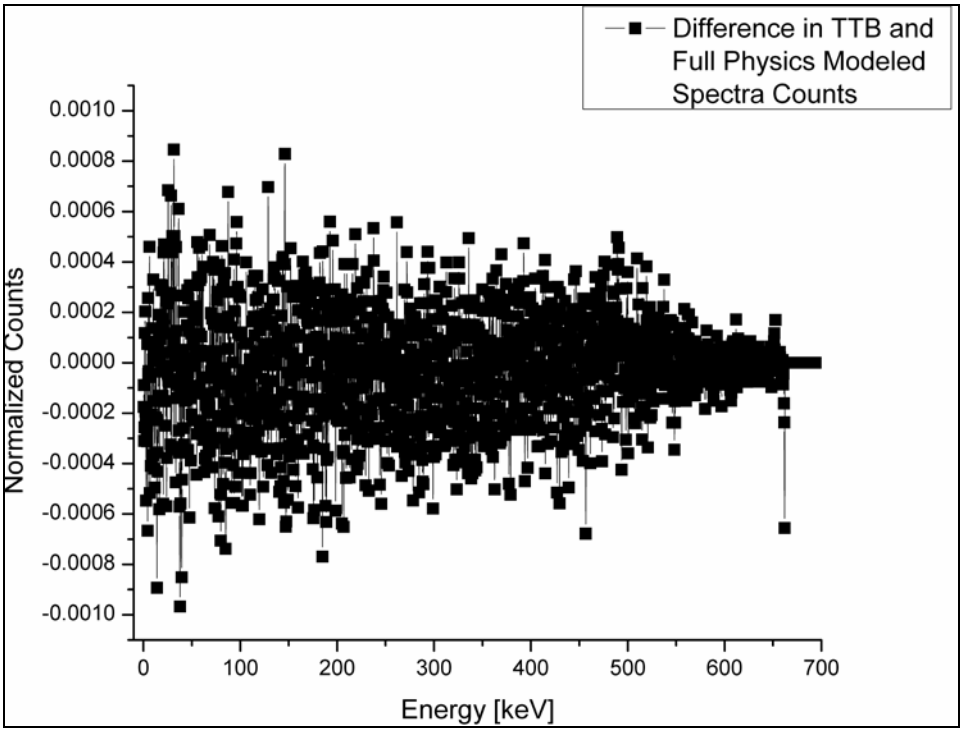

Figure 15. Difference in Counts between TTB and Full Physics Modeled Spectra.

The DRFs generated in MCNP all have a detector-to-source distance of 50 cm. In addition, they all have a concrete scattering plane and use the TTB model. The DRFs also have an energy cutoff of 1 keV, so that gammas below that energy would be disregarded. The DRFs use energy bins of 1 keV and were created for energies of 20 keV, 50 keV, 100 keV, and every 50 keV thereafter up through 3000 keV, as required by

the current version of ASEDRA. A sample MCNP DRF input file is shown in Appendix D.

3.4 Experimental Setup

The sources used in this experiment were solid samples of Cd-109, Co-57, Eu-152 and solutions of Sb-125, Eu-154, and Eu-155. The certificates of calibration files for these sources are given in Appendices E, F, C, and G respectively. All measurements were performed in the secure computing room with the sources 50 cm from the detector. Figure 16 shows how the sources were mounted on a wooden block in order for the center of the detector to be in line with the sources.

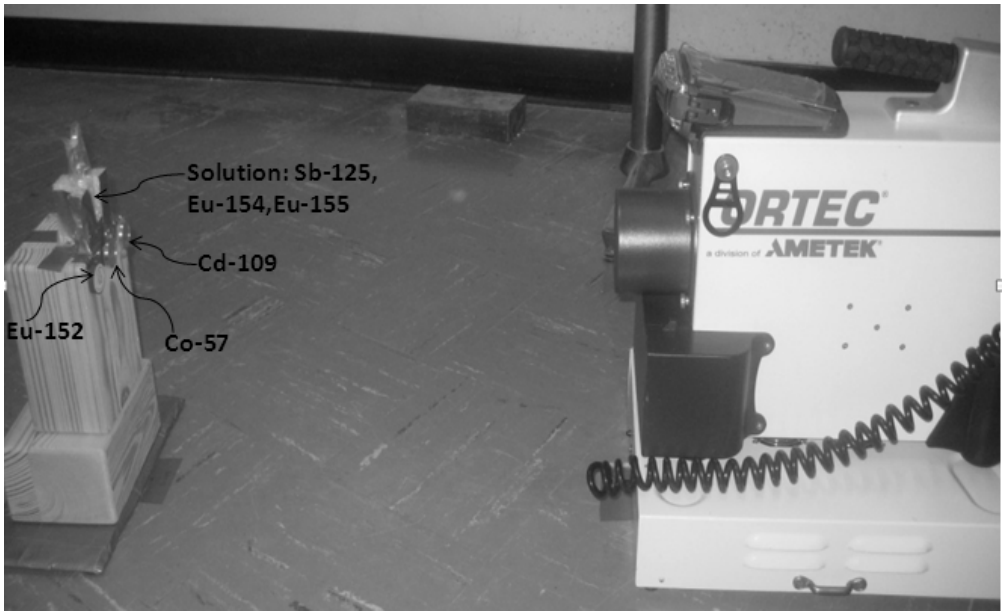

Figure 16. Experimental Setup.

The same sets of measurements were taken ten different times in this configuration. Each of the 10 measurements consisted of 19 various measurement times;

70560, 7200, 3600, 3000, 2400, 1800, 1200, 600, 300, 180, 60, 50, 40, 30, 20, 10, 5, 3, and 1 second. The spectra from one set of measurements are shown in Appendix H.

As well as the measurements taken with all sources, there were five sets of measurements taken with only the solution of the Sb-125, Eu-154, and Eu-155 sources. This was done because the sources in the solution were much weaker than the Co-57, Eu-152, and Cd-109 sources and it needed to be determined which peaks were actually measured when the solution was measured alone. The 5 measurements of the solution were all taken for the same 19 time intervals that were used with the measurements of all the sources.

3.5 Explanation of Comparison Parameters

Following the experimental measurements, the spectra collected were analyzed using Genie™ and ASEDRA. To apply these programs to the spectra, a few parameters had to be defined in order to provide a baseline for comparison. The ground truth is defined as the 31 peaks that are present in the spectra based on the sources used in the experiment and are shown in Table 4 [22]. The probability per decay for each of the ground truth gamma-ray peaks are given in Appendix I [23].

The number of positive peaks that either program identifies is defined as the number of peaks the program identifies that are ground truth peaks. The number of false positive peaks that either program identifies is defined as the number of peaks that are not ground truth peaks that the program identifies. To ensure that each program is applied with its optimal conditions, the parameters of both Genie™ and ASEDRA were optimized for each time measurement. This provided a commonality between the two programs for

using the number of positive and false positive peaks found as a comparison. Genie™ is used in this experiment as a benchmark for comparison to ASEDRA. The goal of this experiment is determine if ASEDRA provides improvements to specificity and sensitivity and that is accomplished by comparing ASEDRA to the benchmark. The optimization process for both Genie™ and ASEDRA is explained in the next two sections.

Table 4. Ground Truth Gamma-Ray Peaks [22].

Nuclide	Energy (keV)	Nuclide	Energy (keV)
Eu-155	45.30	Eu-152	778.89
Eu-152	45.40	Eu-152	867.32
Eu-155	86.55	Eu-154	873.19
Cd-109	88.03	Eu-152	964.01
Eu-152	121.78	Eu-154	996.32
Co-57	122.06	Eu-154	1004.80
Eu-154	123.07	Eu-152	1085.80
Co-57	136.48	Eu-152	1089.70
Eu-152	244.69	Eu-152	1112.00
Eu-154	247.94	Eu-152	1212.80
Eu-152	344.28	Eu-154	1274.44
Eu-152	411.11	Eu-152	1299.00
Eu-152	443.98	Eu-152	1408.01
Eu-154	692.41	Eu-154	1593.00
Eu-154	723.30	Eu-154	1596.50
Eu-154	756.87		

3.6 Genie™ Optimization and Implementation

To determine the optimal settings for Genie™, the number of positive peaks was maximized, and the number of false positive peaks minimized. The Genie™ parameters adjusted to do so were the Peak Search Sensitivity (PSS) and the Gaussian Sensitivity (GS). The PSS is the number of standard deviations above background a feature must be

to be considered a peak. The GS determines how close to a pure Gaussian shape a peak should be.

The optimal settings for these parameters were determined for each time measurement, from one set of measurements with the background removed. The PSS was initially set at 3 and held constant while the GS varied from 1 to 40. The number of positive and false positive peaks was recorded for each GS value. After this was completed a threshold analysis was utilized to verify which GS value maximized the number of positive peaks while minimizing the number of false positive peaks. The threshold analysis consisted of examining how the quantity of positive and false positive peaks changed with varying values of the GS and determining the threshold at which the number of positive peaks was at the greatest number it could be while continuing to keep the amount of false positive peaks at a minimum. The PSS was then varied from 1 to 40 while the GS was kept constant. The number of positive and false positive peaks was evaluated for each PSS value. The threshold analysis was then applied to verify the value of PSS that maximized the number of positive peaks while minimizing the number of false positive peaks. Once the best PSS value was found, the entire data set was again analyzed while varying the GS from 1 to 40 to see if there is a better GS value based on the PSS value. This entire process was repeated until the optimal GS and PSS parameters were established for each time measurement. The result of this process is shown in Table 5.

Table 5. Genie™ Peak Search Sensitivity and Gaussian Sensitivity Optimal Settings

Time Measurement (sec)	Peak Search Sensitivity	Gaussian Sensitivity
1	1	10
3	2	10
5	2	10
10	2.3	10
20	2.8	10
30	3	10
40	4	10
50	3	30
60	2.8	13
180	3.2	1
300	3.9	10
600	3.1	14
1200	3.3	15
1800	3.5	5
2400	3.8	15
3000	4	30
3600	5	40
7200	6	10
70560	18	10

3.7 ASEDRA Optimization and Implementation

To establish the optimal settings for ASEDRA, the quantity of positive peaks was to be maximized while minimizing the number of false positive peaks. The ASEDRA parameters modified were the peak aliasing and alpha. The peak aliasing factor allows a sweeping of the spectra, aliasing peaks that are too close to other central peaks. This allows for small incidental peaks to be removed and summed into a neighboring 'locally dominant' peak. The aliasing factor defines the number of FWHM widths, at a particular energy, considered surrounding above or below prominent peaks. The alpha factor controls the performance of adaptive ACHIP denoising. As the value of alpha is decreased, the denoising increases.

To determine the best settings for these parameters, a similar process as described for the Genie™ optimization was completed. The peak aliasing was initially set at 1 and was held constant while alpha varied from 0 to 1. The number of positive and false positive peaks found was recorded for each alpha value. After this was finished a threshold analysis was employed to find which alpha value maximized the number of positive peaks while minimizing the quantity of false positive peaks. The threshold analysis consisted of examining how the number of positive and false positive peaks changed with varying values of the alpha and resolving the threshold at which the number of positive peaks was at its greatest amount while continuing to keep the number of false positive peaks at a minimum. The peak aliasing was then varied from 0 to 100 while alpha remained constant. The quantity of positive and false positive peaks was determined for each peak aliasing value. The threshold analysis was then applied to establish the peak aliasing value that maximized the number of positive peaks while minimizing the number of false positive peaks. Once the best peak aliasing value was found, the process was repeated using that peak aliasing value and varying alpha from 0 to 1 again, to verify if there is a better alpha value based on the new peak aliasing value. This complete process was repeated until the optimal alpha and peak aliasing parameters were established for each time measurement. This is shown in Table 6.

Table 6. ASEDRA Peak Aliasing and Alpha Optimal Settings.

Time Measurement (sec)	Peak Aliasing	Alpha
1	0.10	no denoising
3	0.10	0.006
5	0.10	0.085
10	0.19	0.995
20	0.45	0.015
30	0.45	0.995
40	0.45	0.995
50	0.50	0.500
60	0.45	0.006
180	0.50	0.022
300	0.50	0.100
600	0.50	0.007
1200	0.80	0.005
1800	0.70	0.008
2400	0.60	0.006
3000	0.50	0.006
3600	1.00	0.020
7200	0.95	0.008
70560	1.00	0.006

IV. Results and Analysis

4.1 Application of Genie™ Results and Analysis

Using the optimal settings, Genie™ was used to process the spectra from the ten measurements at all nineteen measurement times and positive and false positive peaks recorded. The Genie™ peak analysis report that is generated gives an abundance of information concerning the peaks as shown in Appendix J. Sample Genie™ Peak Analysis ReportAppendix J. However, for this analysis only the number of peaks located and the energy at which those peaks are located was used. This is because the objective of this research was to determine if the application of ASEDRA resulted in improvements in specificity and sensitivity. To achieve this objective, the ability to apply ASEDRA to locate ground truth peaks was benchmarked by comparing it to Genie™.

In order for one of the Genie™ located peaks to be considered a positive peak, its energy was required to be within 2% of the ground truth energy, as shown in Table 4. This parameter was chosen as a metric to establish which peaks are in-fact ground truth peaks and as a way to consistently define positive and false positive peaks for the duration of the analysis. This 2% metric was based on several factors, the first and most important being that the largest resolution of the HPGe detector is approximately 2%. Next, the energy calibration ranged from 0.11-0.38 keV, 0.02-0.22%, of their known values, so the metric establishing whether or not a peak was considered to be a ground truth peak needed to be greater than this. Lastly, the change in the calibration and experimental background only varied by 0.07 and 1.7% respectively throughout the experiment, which supports using the 2% metric to determine which peaks are ground

truth peaks. By means of this 2% bound, positive peaks are located in the spectra from the 10 measurements at all 19 measurement times. The compilation of this data is shown in Table 7 where 'x' denotes that a ground truth peak for that row was located, in at least 5 of the 10 measurements, at that particular measurement time.

Table 7. Genie™ Located Peaks based on all Ten Measurements.

		Measurement Time (sec)																		
Nuclide	Energy (keV)	1	3	5	10	20	30	40	50	60	180	300	600	1200	1800	2400	3000	3600	7200	70560
Eu-155	45.30																			
Eu-152	45.40											x	x	x	x	x	x	x	x	x
Eu-155	86.55												x		x	x			x	x
Cd-109	88.03	x	x	x	x	x	x	x	x	x	x	x	x	x	x	x	x	x	x	x
Eu-152	121.78	x	x	x	x	x	x	x	x	x	x	x	x	x	x	x	x	x	x	x
Co-57	122.06																			
Eu-154	123.07																			
Co-57	136.48			x	x	x	x	x	x	x	x	x	x	x	x	x	x	x	x	x
Eu-152	244.69		x	x	x	x	x	x	x	x	x	x	x	x	x	x	x	x	x	x
Eu-154	247.94													x	x	x	x	x	x	x
Eu-152	344.28	x	x	x	x	x	x	x	x	x	x	x	x	x	x	x	x	x	x	x
Eu-152	411.11					x	x	x	x	x	x	x	x	x	x	x	x	x	x	x
Eu-152	443.98					x	x	x	x	x	x	x	x	x	x	x	x	x	x	x
Eu-154	692.41												x	x	x	x	x	x	x	x
Eu-154	723.30												x	x	x	x	x	x	x	x
Eu-154	756.87																			
Eu-152	778.89			x	x	x	x	x	x	x	x	x	x	x	x	x	x	x	x	x
Eu-152	867.32						x	x	x	x	x	x	x	x	x	x	x	x	x	x
Eu-154	873.19													x	x	x	x		x	x
Eu-152	964.01			x	x	x	x	x	x	x	x	x	x	x	x	x	x	x	x	x
Eu-154	996.32													x	x	x	x	x	x	x
Eu-154	1004.80										x	x	x	x	x	x	x	x	x	x
Eu-152	1085.80				x	x	x	x	x	x	x	x	x	x	x	x	x	x	x	x
Eu-152	1089.70										x	x	x	x	x	x	x	x	x	x
Eu-152	1112.00				x	x	x	x	x	x	x	x	x	x	x	x	x	x	x	x
Eu-152	1212.80										x	x	x	x	x	x	x	x	x	x
Eu-154	1274.44										x	x	x	x	x	x	x	x	x	x
Eu-152	1299.00										x	x	x	x	x	x	x	x	x	x
Eu-152	1408.01				x	x	x	x	x	x	x	x	x	x	x	x	x	x	x	x
Eu-154	1593.00																			
Eu-154	1596.50																			x

In order to determine the trends in the number of positive and false positive peaks that Genie™ identifies, the average number of peaks found in each of the ten measurements was taken. Along with that, the average deviation was calculated for each time measurement as shown in Equation (10). This average deviation gives the average of the absolute values of the deviations of the data points from their mean and is a measure of the variability in the data set.

$$\frac{1}{n}\sum\left|x-\bar{x}\right| \tag{10}$$

The average number of positive peaks that Genie™ found at each measurement time is plotted in Figure 17 with the error bars indicating the average deviation.

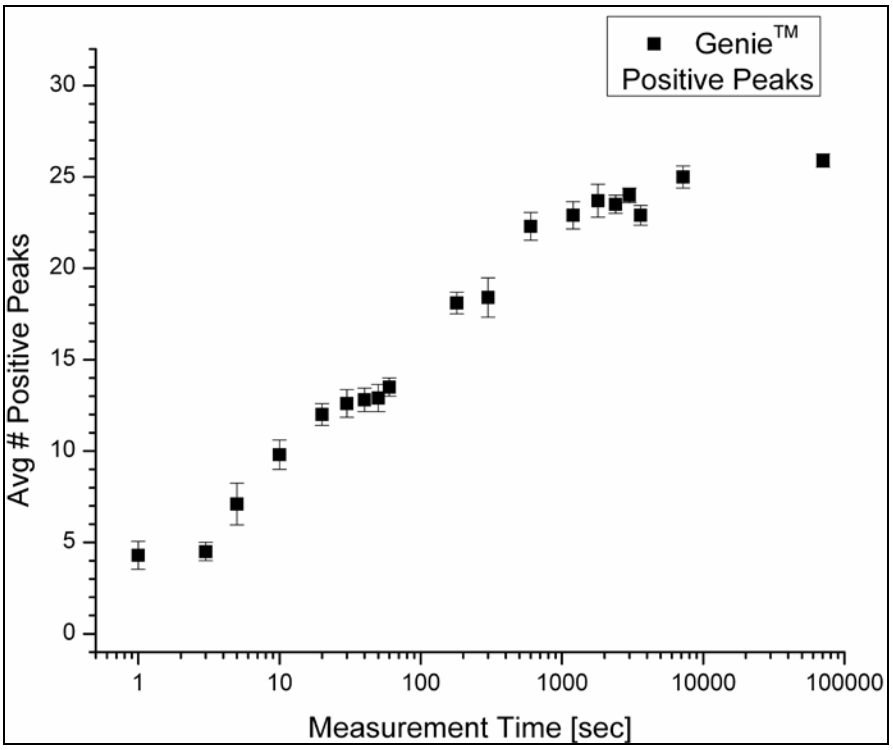

Figure 17. Genie™ Located Positive Peaks.

Figure 17 illustrates that the number of positive peaks increases as the measurement time is raised. It also shows the 1 second measurement time locating the minimum average number of positive peaks at 4.3, and at the 70560 second measurement time Genie™ identifies the maximum average number of positive peaks, that being 25.9 out of the possible 31 ground truth peaks. This behavior is expected due to the ability to collect additional spectral information as more detection time is allotted. The average deviation remains very small for all time measurements with 0.36 being the smallest and occurring at the 70650 second time measurement and 1.14 being the largest taking place at the 5 second time measurement. This demonstrates that the number of Genie™ located

positive peaks do not vary significantly between the 10 separate measurements that were taken.

The number of false positive peaks identified using Genie™ was also examined and is plotted in Figure 18 with the error bars indicating the average deviation.

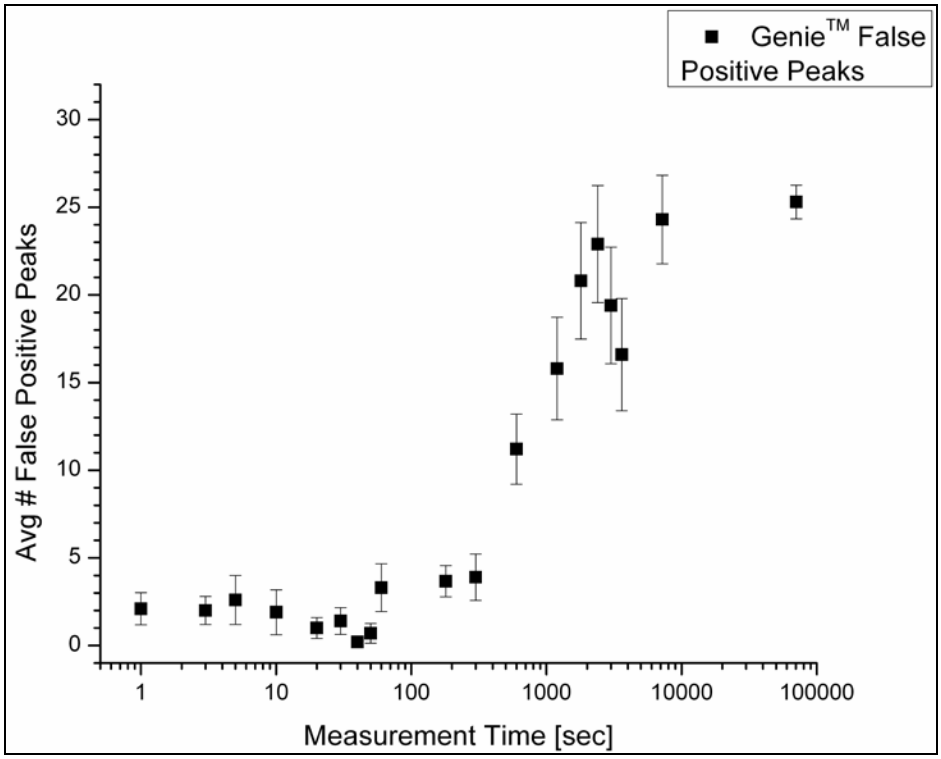

Figure 18. Genie™ Located False Positive Peaks.

Figure 18 shows a general trend of increase in the quantity of false positive peaks that Genie™ locates as the measurement time becomes longer, especially after about 100 seconds. In addition, the minimum and maximum average number of false positive peaks is 0.2 at the 40 second time measurement and 25.3 at the 70560 second time measurement. This behavior is slightly different than that of the positive peaks that

Genie™ locates, given that the minimum average number of false positive peaks found is at the 40 second measurement, instead of the 1 second measurement for the positive peaks. This can be attributed back to adjusting the Genie™ parameters to achieve the best performance. This required occasionally accepting more false positive peaks in order to get additional positive peaks, as shown in the time measurements below the 40 second time measurement. The average deviation stays fairly small for the time measurements at and below 300 seconds and at 70560 seconds. The average deviation in the measurement time range of 600 to 7200 seconds is somewhat larger. The smallest average deviation is 0.32 and occurs at the 40 second time measurement and 3.34 is the largest taking place at the 2400 second time measurement. This demonstrates that the number of Genie™ located false positive peaks demonstrate the most variance in the time measurement range of 600 to 7200 seconds.

In order to conclude the analysis of the peak finding capability of Genie™ and compare it to the capability of ASEDRA, a metric was implemented that included both the positive and false positive peaks. This is accomplished by applying Equation (11) to each time measurement.

$$PerformanceParameter = \frac{\#PositivePeaks - \#FalsePositivePeaks}{\#GroundTruthPeaks} \qquad (11)$$

The best performance of Genie™ consists of finding all of the ground truth peaks while not locating any false positive peaks. When this occurs the performance will be equal to 1. The closer the performance parameter is equal to 1, the better that Genie™ is

performing. Also, when the performance parameter goes negative, the number of false positive peaks is exceeding the number of positive peaks which signifies that Genie™ is not performing very well. The performance parameter of Genie™ at all 19 time measurements, calculated for each of the ten measurements then averaged, is illustrated in Figure 19.

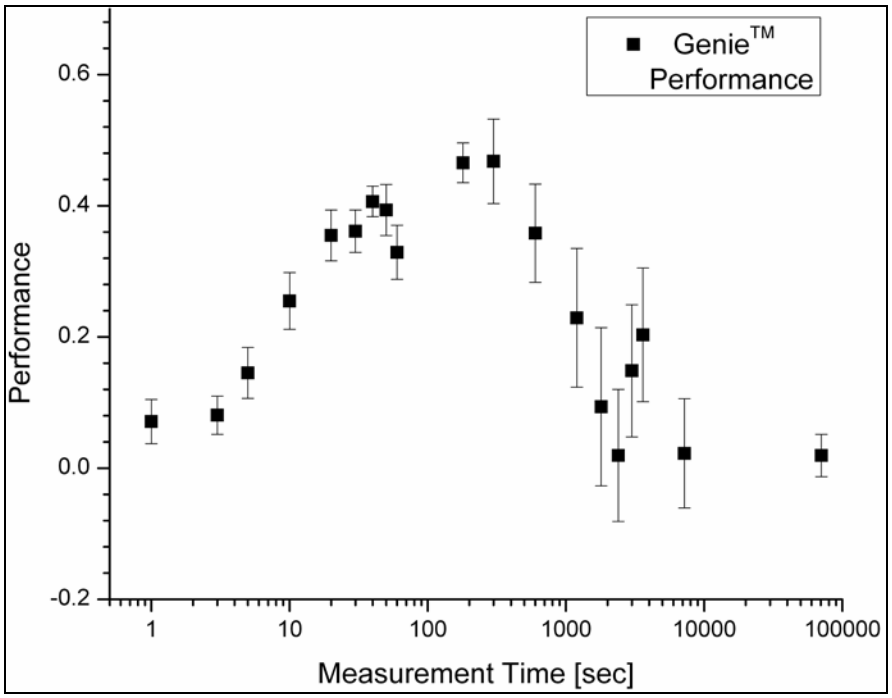

Figure 19. Genie™ Performance.

Figure 19 shows that the best performance of Genie™ is 0.47 which occurs at the 300 second time measurement and the worst performance of Genie™ is 0.02 which takes place at the 2400 second time measurement. Genie™ working the best at the 300 second time measurement is reasonable based on the longer counting time which allows for a reasonable number of peaks to be seen without being so long that artificial peaks begin

emerging. The poorest performance of Genie™, which occurs at the 2400 second time measurement, can be attributed to the large number of false positive peaks that appear due to the longer counting time. The trend on the performance of Genie™ does not just simply increase or decrease in relationship with the measurement time. The trend starts off with the performance increasing with counting time, but after the 300 second measurement, the performance starts to decrease. This decline in performance continues until it bottoms out at the 2400 second measurement. The performance then begins to increase again up until the 3600 second measurement time at which it drops yet again for the 7200 measurement and stays constant for the 70560 second measurement.

Overall the performance of Genie™ is the best at the middle measurement times and worst at the short and long measurement times. The largest average deviation for the performance is 0.12 and occurs at the 1800 second measurement with the smallest performance average deviation being 0.02 and happening at the 40 second measurement. These variations in the average deviation are based on the counting times. Figure 19 illustrates the average deviation being small at short and the longest counting times, and being large in between.

4.2 Application of ASEDRA Results and Analysis

The optimal settings established for ASEDRA were applied to the spectra from the 10 measurements at each of the 19 various measurement times. The peak analysis report that ASEDRA produces provides only the energy at which the peak occurs and the number of counts in that peak as shown in Appendix K. In this analysis, the energy at which the peak is located is the only piece of information provided and used. For an

ASEDRA located peak to be considered a positive peak, its energy has to be within 2% of the ground truth energy as shown in Table 4, just as in the case with Genie™. Using this 2%, the number of the positive peaks was determined and these results are shown in Table 8.

Table 8. ASEDRA Located Peaks based on all Ten Measurements.

		Measurement Time (sec)																		
Nuclide	Energy (keV)	1	3	5	10	20	30	40	50	60	180	300	600	1200	1800	2400	3000	3600	7200	70560
Eu-155	45.30																			
Eu-152	45.40																	x	x	x
Eu-155	86.55																			
Cd-109	88.03				x	x	x	x	x	x	x	x	x	x	x	x	x	x	x	x
Eu-152	121.78	x	x	x	x	x	x	x	x	x	x	x	x	x	x	x	x	x	x	x
Co-57	122.06		x	x	x															
Eu-154	123.07																			
Co-57	136.48				x	x	x	x	x	x	x	x	x	x	x	x	x	x	x	x
Eu-152	244.69				x	x	x	x	x	x	x	x	x	x	x	x	x	x	x	x
Eu-154	247.94																			x
Eu-152	344.28			x	x	x	x	x	x	x	x	x	x	x	x	x	x	x	x	x
Eu-152	411.11										x	x	x	x	x	x	x	x	x	x
Eu-152	443.98										x	x	x	x	x	x	x	x	x	x
Eu-154	692.41													x	x	x	x	x	x	x
Eu-154	723.30															x	x	x	x	x
Eu-154	756.87																			
Eu-152	778.89						x	x	x	x	x	x	x	x	x	x	x	x	x	x
Eu-152	867.32										x	x	x	x	x	x	x	x	x	x
Eu-154	873.19																			x
Eu-152	964.01						x	x	x	x	x	x	x	x	x	x	x	x	x	x
Eu-154	996.32																		x	x
Eu-154	1004.80												x	x	x	x	x	x	x	x
Eu-152	1085.80							x	x	x	x	x	x	x	x	x	x	x	x	x
Eu-152	1089.70												x	x	x	x	x	x	x	x
Eu-152	1112.00						x	x	x	x	x	x	x	x	x	x	x	x	x	x
Eu-152	1212.80												x	x	x	x	x	x	x	x
Eu-154	1274.44													x	x	x	x	x	x	x
Eu-152	1299.00												x	x	x	x	x	x	x	x
Eu-152	1408.01						x	x	x	x	x	x	x	x	x	x	x	x	x	x
Eu-154	1593.00																			
Eu-154	1596.50																			x

In order to calculate the number of positive and false positive peaks identified using ASEDRA, the average of the 10 measurements was taken. In addition, the average deviation is calculated for each time measurement as given in Equation (10). The average number of positive peaks that ASEDRA locates for each time measurement is plotted in Figure 20, with the error bars indicating the average deviation.

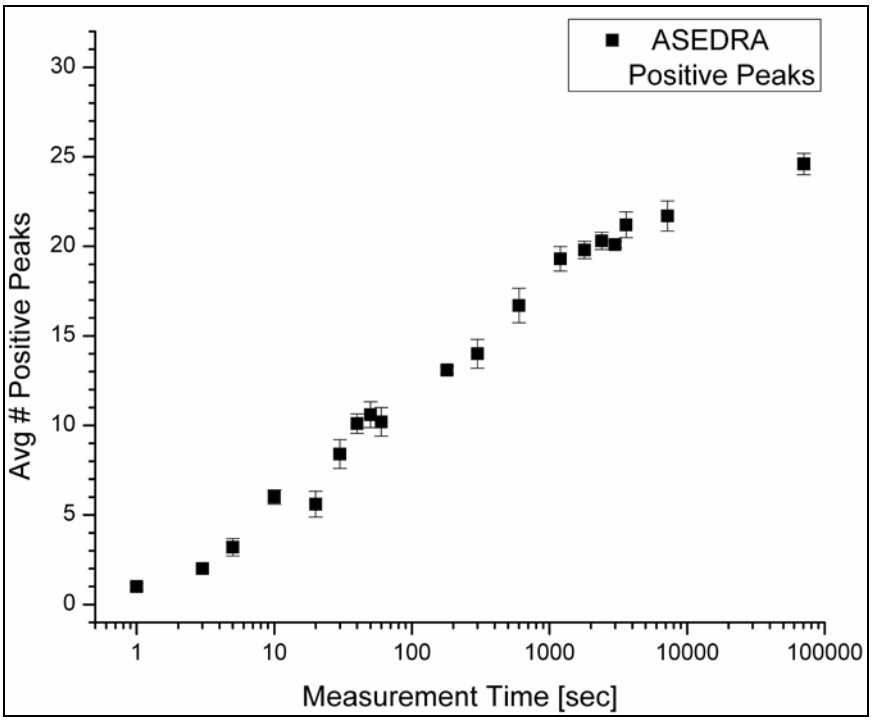

Figure 20. ASEDRA Located Positive Peaks.

Figure 20 shows a general trend of the average number of positive peaks increasing as the measurement time is increased. The minimum average amount of positive peaks that ASEDRA locates is 1 at the 1 second measurement and the maximum average number of peaks that ASEDRA can locate is 24.6 at the 70560 second measurement. This behavior is anticipated based on the increased detection time

providing extra spectral information. The average deviation stays small for all the time measurements where the smallest is 0 and occurs at the 3 second time measurement and the largest is 0.96 and occurs at the 600 second time measurement. This reveals that the number of positive peaks identified using ASEDRA locates does not have much variation among the ten separate measurements that were taken.

The average number of the false positive peaks that ASEDRA located is shown in Figure 21 with the error bars again signifying the average deviation.

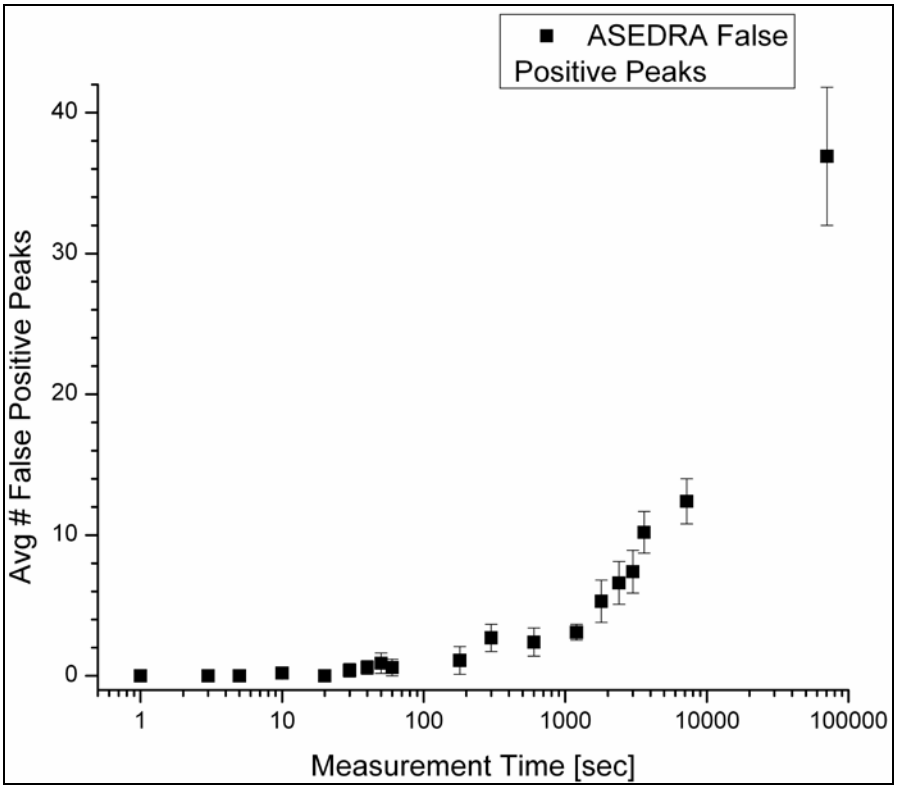

Figure 21. ASEDRA Located False Positive Peaks.

Figure 21 illustrates a trend of an increase in the number of false positive peaks that ASEDRA locates as the measurement time is raised, especially after about 100

seconds. The minimum and maximum average number of false positive peaks that ASEDRA locates is 0 at the 1, 3, 5 and 20 second time measurements and 36.9 at the 70560 second time measurement. This behavior follows that of the positive peaks that ASEDRA locates, given the increase in located peaks with the addition of measurement time. This can be attributed to the additional spectral information gained with more detection time. The average standard deviation remains rather small for the time measurements at and below 60 seconds and at 1200 seconds. The average deviation, in the measurement time range of 180 to 7200 seconds is slightly larger and is the greatest at the 70560 time measurement. The smallest average deviation is 0 and occurs at the 1, 3, 5, and 20 second time measurements and 4.9 is the largest taking place at the 70560 second time measurement. This shows that the false positive peaks ASEDRA located have the most variance in the range of the 180 to 70560 second time measurements, for the 10 separate measurements that were taken.

The performance of ASEDRA was calculated by applying Equation (11), which was also applied to determine the performance of Genie™. The best performance of ASEDRA is based on locating every ground truth peak while not finding any false positive peaks. When this takes place the performance parameter will be equal to 1. The closer the performance parameter is to 1, the better ASEDRA is performing. In addition, when the performance parameter becomes negative, the quantity of false positive peaks are greater than the number of positive peaks which indicates that ASEDRA is not performing well. The average performance of ASEDRA at each of 19 time measurements is illustrated in Figure 22.

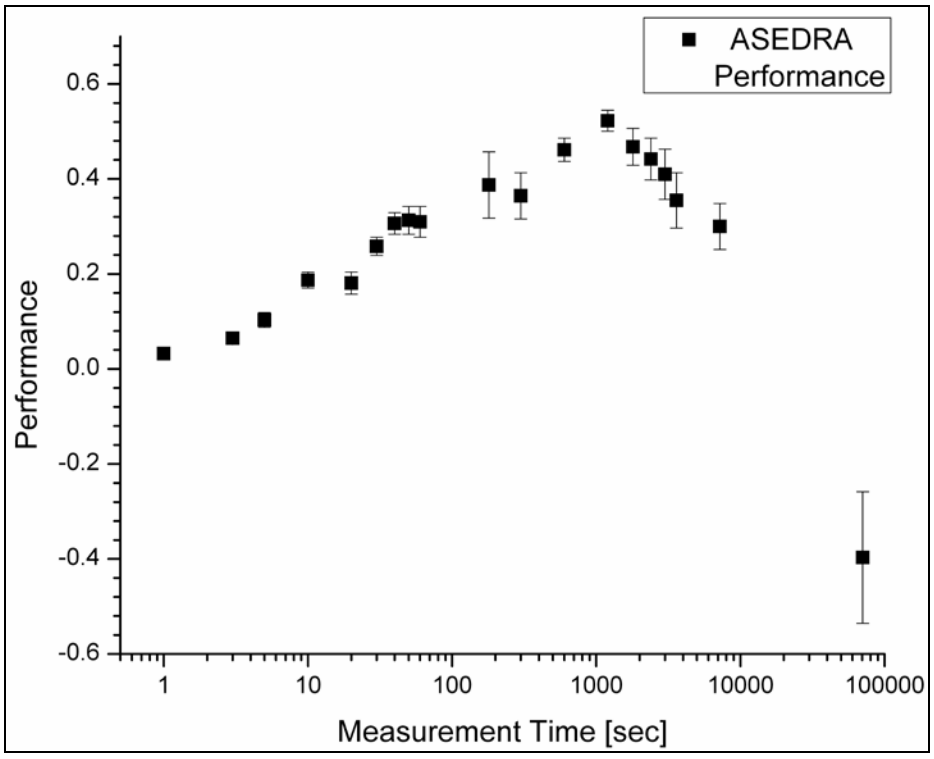

Figure 22. ASEDRA Performance.

Figure 22 illustrates that the best performance of ASEDRA is 0.52 which takes place at the 1200 second time measurement and the worst performance of ASEDRA is -0.40 which occurs at the 70560 second time measurement. The fact that ASEDRA performs the best at the 1200 second time measurement is sensible because the longer counting time results in a larger number of positive peaks without a significant increase in false positive peaks appearing. The 70560 second time measurement has the poorest performance for ASEDRA. Because this is the longest measurement time, one might think it would provide the best performance because it will give the most spectral information. Although this is true, it also offers the possibility for more false positive peaks to appear which is the sole reason why ASEDRA performs the worst at this time

measurement. The performance trend of ASEDRA does not just increase or decrease with relation to the measurement time. The behavior of the performance begins with the performance increasing as counting time goes up, to a maximum at the 1200 second time measurement. The performance then starts to decrease and continues declining until the 70560 time measurement.

In general the performance of ASEDRA is the best at the middle measurement times and worst at the short and long measurement times. The largest average deviation for the performance is 4.9 and happens at the 70560 second measurement with the smallest performance average deviation being 0 and taking place at the 1, 3, 5, and 20 second measurement times. These variations in the average deviation are based on the counting times, with the smallest occurring at short measurement times and the longest happening at the long measurement time.

4.3 Comparison of Genie™ and ASEDRA Results

This section will compare and contrast the application of Genie™ and ASEDRA to the experimental spectra. The optimal settings are being used to compare the application of both methods. This provides a standard of comparison for the two programs. The number of positive peaks that each program locates is shown in Figure 23. This value is the average of the 10 measurements. Also, the error bars indicated the average deviation for each measurement.

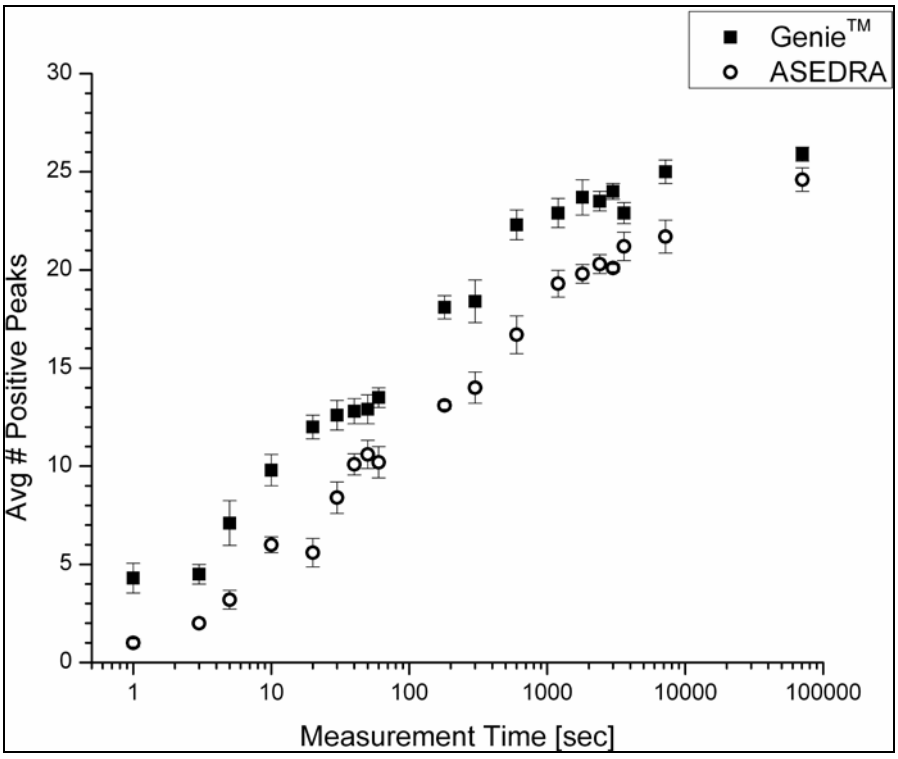

Figure 23. Genie™ and ASEDRA Located Positive Peaks.

As illustrated in Figure 23, both programs demonstrate the same trend in which they locate more positive peaks as the measurement time is increased, a behavior which is expected. Figure 23 also shows that Genie™ locates more positive peaks than ASEDRA at every measurement time. The average maximum number of peaks that Genie™ finds is 25.9, whereas for ASEDRA it is 24.6. The average deviation for both Genie™ and ASEDRA are small for all time measurements, but Genie™ has a larger average deviation than ASEDRA for most of the measurement times. This demonstrates that more variation occurs between the 10 measurements when applying Genie™ versus ASEDRA.

The number of Genie™ and ASEDRA false positive peaks was also examined. The results are illustrated in Figure 24 with the error bars again signifying the average deviation from 10 measurements.

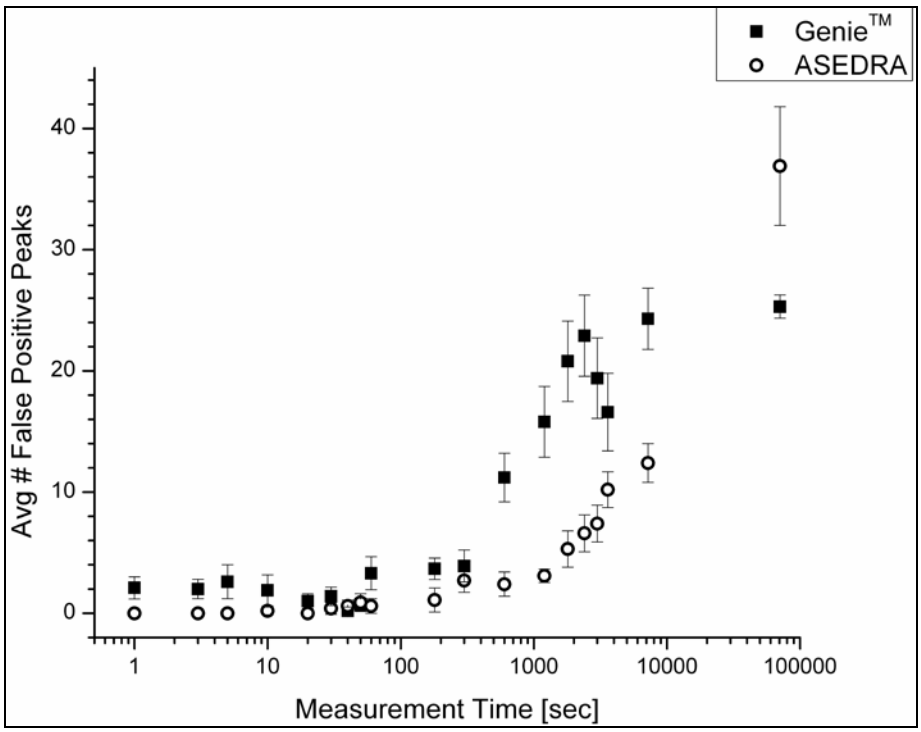

Figure 24. Genie™ and ASEDRA Located False Positive Peaks.

Figure 24 shows an increase in the false positive peaks that are found as the measurement time is raised for both Genie™ and ASEDRA. This behavior is expected because of the added spectral information that comes along with longer detection times. Figure 24 illustrates that Genie™ finds more false positive peaks than ASEDRA at every measurement time except the 40, 50, and 70560 second measurement times. The maximum average number of false positive peaks that Genie™ locates is 25.3, whereas for ASEDRA it is 36.9. The average deviation for both Genie™ and ASEDRA are small

for the shorter measurement times and becomes larger as the measurement time is increased. Generally speaking the average deviation is larger for the Genie™ measurements than for ASEDRA, but the largest average deviation occurs for ASEDRA at the 70560 second measurement time.

The particular ground truth peaks that Genie™ and ASEDRA are able to locate are examined. The 4 ground truth peaks that neither program locates, meaning they do not appear in at least five of the ten measurements, are shown in Table 9. The reason that the 45.30 and 123.07 keV peaks are never located can be attributed to these peaks being very close in energy, within one percent, to other ground truth peaks, and neither program resolved these peaks. Additionally, the 756.87 and 1593.00 keV peaks were not found owing to their small activity as shown in Appendix I.

Table 9. Ground Truth Peaks Never Located by Genie™ or ASEDRA.

Nuclide	Energy (keV)
Eu-155	45.30
Eu-154	123.07
Eu-154	756.87
Eu-154	1593.00

In addition there are ground truth peaks that one program finds, but the other one does not locate. Genie™ finds the Eu-155 86.55 keV peak which ASEDRA is never able to locate and ASEDRA finds the Co-57 122.06 keV and Genie™ is never able to locate that peak. Genie™ is able to discern the Eu-155 86.55 keV peak from the Cd-109 88.03 keV peak and ASEDRA is able to resolve the Co-57 122.06 keV peak from the Eu-152

121.78 keV peak. This shows that both Genie™ and ASEDRA are able to sometimes identify peaks that are close together.

To compare the performance of Genie™ and ASEDRA, Equation (11) is applied to both programs at all 19 time measurements and is illustrated in Figure 25.

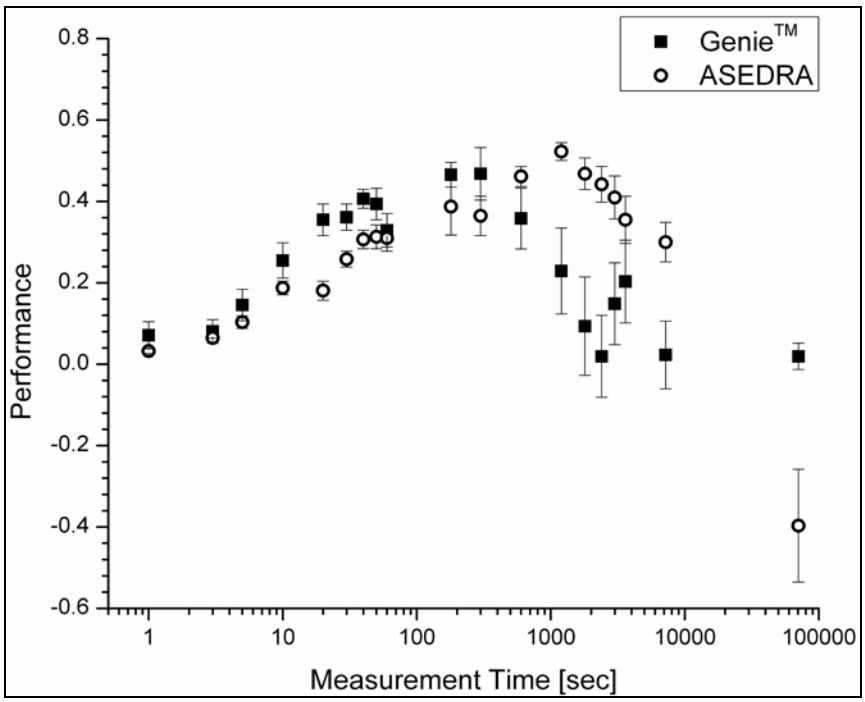

Figure 25. Genie™ and ASEDRA Performance.

Figure 25 shows how the performance of both Genie™ and ASEDRA increases then decreases with measurement time. The performance of Genie™ and ASEDRA increases up until the 1800 second time measurement. For Genie™ it begins to decrease until it levels out at the 70560 second measurement. For ASEDRA, the performance decreases for the remainder of the measurement times, owing to the increasing number of false positives.

For the measurement time range of 1 to 300 seconds, the performance parameter is higher for Genie™ than ASEDRA. For the 600 to 7200 second measurement time range, the performance parameter is for ASEDRA is higher than that of Genie™. Lastly at the 70560 second time measurement, Genie™ has a higher performance parameter than ASEDRA. The largest difference in performance occurs at the 2400 second time measurement in which the performance of ASEDRA is greater than that of Genie™ by 0.42. The smallest difference in performance takes place at the 3 second time measurement in which Genie™ performs better than ASEDRA by 0.02. For Genie™, the highest performance parameter is 0.47 and occurs at the 300 second time measurement. For ASEDRA, the highest performance parameter is 0.52 and occurs at the 1200 second time measurement.

An additional method of comparing the ability of Genie™ and ASEDRA to locate peaks is to use Receiver Operating Characteristic (ROC) curves. These ROC curves plot the percentage of false positive peaks located, (representing $1 - S$, where S is selectivity),

against the percentage of true positive peaks located, sensitivity. The area under the curve becomes greater as the performance increases, maximizing the positive peaks and minimizing the false positive peaks. The ROC curve shown in Figure 26 is for each of the nineteen measurement times for both Genie™ and ASEDRA.

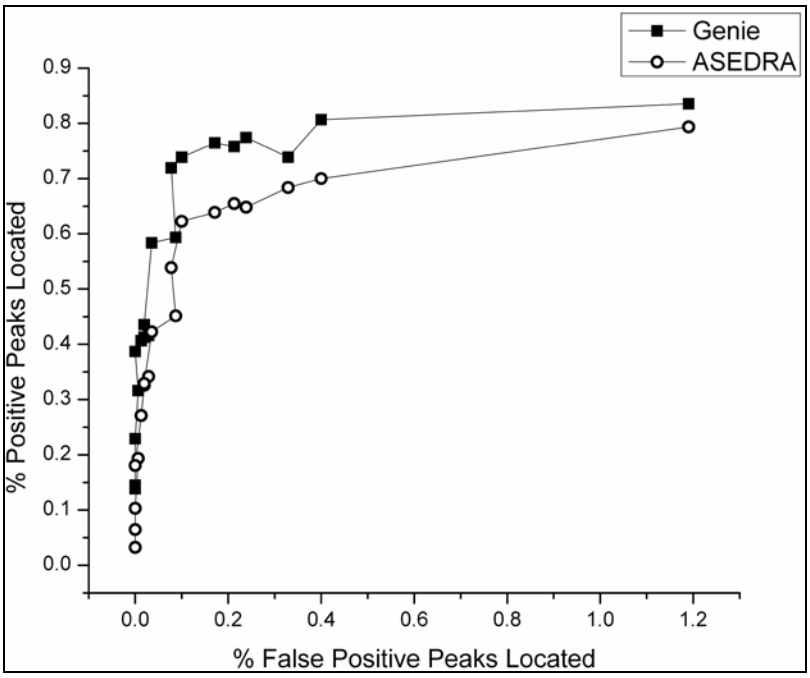

Figure 26. Receiver Operating Characteristic (ROC) Curve for ASEDRA and Genie™.

The ROC curve illustrates a larger area under the curve for Genie™ versus ASEDRA, which indicates that Genie™ is better at maximizing the number of positive peaks it locates while minimizing the number of false positive peaks. Furthermore, it shows that improvement to ASEDRA requires better location of positive peaks, primarily regarding the lower energy peaks, as identified in Table 8. ASEDRA Located Peaks based on all Ten Measurements.

Lastly, another way to compare the two methods is to consider the sum peaks that either program locates. Sum peaks occur from isotopes that emit multiple cascade gamma-rays in its decay. It is then possible for both gamma-ray photons from a single decay to interact and deposit all of their energy into the detector. If enough of these events occur, a sum coincidence peak will be observable in the spectrum that occurs at an

energy which corresponds to the sum of the two individual gamma-rays [7]. The sum peaks were not initially taken into consideration when determining the 31 ground truth peaks, but with the amount of false positive peaks that were identified in both programs, it was deemed necessary. Eu-152 was the only Europium isotope examined based on its activity. Only two sum peaks were investigated, located at 1530 keV and 1650 keV, based on the probabilities for the coincident emission gamma-rays [24]. The spectra from all nineteen time measurements, for both Genie™ and ASEDRA, were examined to determine if either program identified the sum peaks listed above. ASEDRA was able to identify the 1530 keV peak at the 70560, 7200, and 3600 second time measurements and never identified the 1650 keV peak. Genie™ was able to identify the 1530 keV peak at the 70560, 7200, 3600, 3000, 2400, 1800, and 1200 second time measurements and also was never able to identify the 1650 keV peak. This reduces the possibility that ASEDRA was misrepresented by identifying "known" peaks as "false peaks" at later times, where the opposite occurred in the data. However, the inclusion of these peaks as "ground truth" would change the analysis as presented.

V. Conclusions and Recommendations

The purpose of this thesis research was to determine if the application of ASEDRA was able to improve the specificity and sensitivity of spectra collected by the HPGe detector. This could then be used as a prevention mechanism to identify sources prior to an event taking place, in the work of nuclear forensics to better identify fission product gamma peaks in a crowded spectrum, as well as decreasing the amount of time needed to take a measurement. To determine if ASEDRA provided these improvements, a spectrum containing 31 known peaks was measured and the average number of positive and false positive peaks was examined to determine the program performance. These results were compared to that of the gamma spectroscopy software Genie™, which was used as a benchmark in this experiment. The performance parameter used in this research is higher for Genie™ than ASEDRA at measurement times at and below 600 seconds and at 70560 seconds. ASEDRA has a performance parameter higher than Genie™ at measurement times between 1200 and 7200 seconds.

The performance parameter is able to give an overall assessment of each program, but it is important to examine how this relates to improvements in specificity and sensitivity. The highest performance parameter for Genie™ is 0.47 and occurs at the 300 second time measurement and for ASEDRA is 0.52 and occurs at the 1200 second time measurement as illustrated in Figure 25. It is very important to note that the performance parameter peaks at different measurement times for Genie™ and ASEDRA. This is significant because the measurement times at which the performance parameters are the highest demonstrate that very long measurement times are not necessary to maximize the

performance of either program. Although this does not directly show an increase in the required measurement time with the application of ASEDRA, it proves that just because a measurement is taken for a longer time does not mean that it provides better information. In addition, there is a certain threshold in which the performance of both programs begins to decrease, even as measurement time is increased. It is also important to examine how the performance parameter for Genie™ maximizes at a lower measurement time than for ASEDRA. This can be attributed to the contribution of Genie™ locating more false positive peaks than ASEDRA at almost every measurement time and the fact that ASEDRA does not locate lower energy peaks as well as Genie™. The latter seems to be due to restrictions within the algorithm itself. The identification of sum peaks also gives some insight into the ability to locate peaks for both programs. By examining the Eu-152 sum peaks, it is clear to see that Genie™ was able to identify the 1530 keV sum peak at more measurement times than ASEDRA. This can be attributed to the possibility of important spectral information being stripped away with the application of ASEDRA to the spectra.

The results clearly show that Genie™ always locates more ground truth peaks than ASEDRA does as illustrated in Figure 23. The results also show that ASEDRA identifies fewer false positive peaks than Genie™ does at all but three of the measurement times as shown in Figure 24. In addition, the performance parameter of Genie™ is higher than ASEDRA at short measurement times, implying that ASEDRA is not able to provide additional spectral information at shorter measurement times. This reveals that the application of ASEDRA does not offer any improvement to the measurement time

required to gain adequate spectral information. Furthermore, at longer times, ASEDRA may be representing numerical noise that results in added false positive peaks.

The results, relating to the ground truth peaks that each program is able to locate, provide information needed to draw conclusions concerning improvements in resolution. ASEDRA is able to resolve the Eu-152 121.78 keV and Co-57 122.06 keV peaks at three of the short measurement times, but can never resolve the Eu-155 86.55 keV and 88.03 keV peaks. On the other hand, Genie™ can resolve the Eu-155 86.55 keV and 88.03 keV peaks at five of the longer measurement times, but is never able to resolve the Eu-152 121.78 keV, Co-57 122.06 keV and 123.07 keV peaks. This demonstrates that applying ASEDRA to the experimental spectra does not bring about an improved accuracy as compared with that of Genie™.

The application of ASEDRA to experimental spectra does not provide any improvements in specificity and sensitivity, as compared to Genie™. With this being said, at longer measurement times ASEDRA was able to better identify ground truth peaks, while minimizing the location of false positive peaks, than Genie™. This demonstrates that the performance of ASEDRA is better than that of Genie™ for longer measurement times, based on the performance parameter. Additionally, ASEDRA found fewer false positive peaks than Genie™ at all but three measurement times. This shows that the application of ASEDRA is superior in not identifying false positive peaks as compared to the application of Genie™. Therefore there is potential for improvements that may make this use of ASEDRA appropriately applicable for use with HPGe detectors.

Recommendations for future work would first include changes to the DRFs. The DRFs used in this experiment were created for energies of every 50 keV, based on the specifications of ASEDRA being written for its initial application with NaI(Tl) detectors. The use of DRFs at energies of every 1 keV would better fit the application of the HPGe at low and high energies, where the linear interpolation fit reduces applicability fo the DRFs. It is not known how this may affect the overall response, but has significant potential in the lower energy region, where stripping has already increased inaccuracies from numerical and statistical noise dominates. This is further exacerbated in this study because the resolution of the HPGe detector is less than 2%, whereas for a NaI(Tl) detector it is in the range of 5-10 %.

Other recommendations pertain to the actual research data set. This problem was made difficult owing to the significant difference in the way ASEDRA and Genie present the results. Taking more than 10 measurements at the 19 different measurement times may provide a more accurate assessment of the peaks that are located as well as present less variation in the experimental measurements. Also developing a metric for the certainty of Genie™ or ASEDRA locating a peak instead of just whether either program finds a peak at least half of the time may be useful, but would require information about the fitting process and accuracy of the fit for each peak in ASEDRA. This would offer more quantitative data regarding how Genie™ and ASEDRA compare.

Lastly, including the sum peaks in the DRFs would remove statistical noise when the source produces coincident decays. Both Genie™ and ASEDRA identified several

false positive peaks at longer measurement times suggesting potential sum peaks from coincident events.

Appendix A. Multi-Nuclide Certificate of Calibration File

Isotope Products Laboratories
An Eckert & Ziegler Company

24937 Avenue Tibbitts
Valencia, California 91355

Tel 661•309•1010
Fax 661•257•8303

T-119

CERTIFICATE OF CALIBRATION
MULTINUCLIDE STANDARD SOURCE

Customer:	WRIGHT PATTERSON AFB	**Source No.:**	1217-4-2
P.O. No.:	IA3206PS217/VISA	**Reference Date:**	1-Nov-06 12:00 PST
Catalog No.:	GF-ML	**Contained Radioactivity:**	1.028 µCi 38.04 kBq

Physical Description:

A. Capsule type: D (25.4 mm OD x 6.35 mm THK)
B. Nature of active deposit: Evaporated metallic salts
C. Active diameter/volume: 5 mm
D. Backing: Epoxy
E. Cover: Acrylic

Gamma-Ray Energy (keV)	Nuclide	Half-life	Branching Ratio (%)	Activity (µCi)	Gammas per second	Total Uncert.
60	Am-241	432.17 ± 0.66 years	36.0	0.02839	378.2	3.3 %
88	Cd-109	462.6 ± 0.7 days	3.63	0.4102	550.9	3.1 %
122	Co-57	271.79 ± 0.09 days	85.6	0.01582	501.1	3.2 %
166	Ce-139	137.640 ± 0.023 days	79.9	0.02069	611.7	3.2 %
279	Hg-203	46.595 ± 0.013 days	81.5	0.06115	1844	3.0 %
392	Sn-113	115.09 ± 0.04 days	64.9	0.08478	2036	3.1 %
514	Sr-85	64.849 ± 0.004 days	98.4	0.09881	3597	3.0 %
662	Cs-137	30.17 ± 0.16 years	85.1	0.07009	2207	3.1 %
898	Y-88	106.630 ± 0.025 days	94.0	0.1595	5547	3.0 %
1173	Co-60	5.272 ± 0.001 years	99.86	0.07905	2921	3.1 %
1333	Co-60	5.272 ± 0.001 years	99.98	0.07905	2924	3.1 %
1836	Y-88	106.630 ± 0.025 days	99.4	0.1595	5866	3.0 %

Method of Calibration:

This source was assayed using gamma ray spectrometry.

Notes:

- See reverse side for leak test(s) performed on this source.
- IPL participates in a NIST measurement assurance program to establish and maintain implicit traceability for a number of nuclides, based on the blind assay (and later NIST certification) of Standard Reference Materials (as in NRC Regulatory Guide 4.15).
- Nuclear data was taken from IAEA-TECDOC-619, 1991.
- Overall uncertainty is calculated at the 99% confidence level.
- This source has a working life of 1 year.

Daniel James Van Dalsem
Quality Control

18-OCT-06
Date

IPL Ref. No.: 1217-4

ISO 9001 CERTIFIED

Medical Imaging Laboratory
24937 Avenue Tibbitts Valencia, California 91355

Industrial Gauging Laboratory
1800 North Keystone Street Burbank, California 91504

Appendix B. Na-22 Certificate of Calibration File

Isotope Products Laboratories
An Eckert & Ziegler Company

24937 Avenue Tibbitts
Valencia, California 91355

Tel 661·309·1010
Fax 661·257·8303

T-107

CERTIFICATE OF CALIBRATION
GAMMA STANDARD SOURCE

Radionuclide:	Na-22	**Customer:**	AIR FORCE INSTITUTE OF TECHNOLOGY/ENP
Half-life:	950.8 ± 0.9 days	**P.O. No.:**	IA3003P084
Catalog No.:	GF-022-M	**Reference Date:**	15-Feb-03 12:00 PST
Source No.:	971-28-2	**Contained Radioactivity:**	0.8796 µCi 32.55 kBq

Physical description:

A. Capsule type:	M (25.4 mm OD x 3.18 mm THK)
B. Nature of active deposit:	Evaporated metallic salt
C. Active diameter/volume:	3 mm
D. Backing:	9.23 mg/cm² kapton
E. Cover:	0.254 mm aluminized mylar

Radioimpurities:

None detected

Method of Calibration:

This source was assayed using gamma ray spectrometry.

Peak energy used for integration:	1275 keV
Branching ratio used:	0.9994 gammas per decay

Uncertainty of Measurement:

A. Type A (random) uncertainty:	± 0.8 %
B. Type B (systematic) uncertainty:	± 3.0 %
C. Uncertainty in aliquot weighing:	± 0.0 %
D. Total uncertainty at the 99% confidence level:	± 3.1 %

Notes:

- See reverse side for leak test(s) performed on this source.
- IPL participates in a NIST measurement assurance program to establish and maintain implicit traceability for a number of nuclides, based on the blind assay (and later NIST certification) of Standard Reference Materials (As in NRC Regulatory Guide 4.15).
- Nuclear data was taken from IAEA-TECDOC-619, 1991.
- This source has a working life of 5 years.

Tuthy Cathum
Quality Control

31 Jan 03
Date Signed

IPL Ref. No.: 971-28

Appendix C. Eu-152 Certificate of Calibration File

Isotope Products Laboratories
An Eckert & Ziegler Company

24937 Avenue Tibbitts
Valencia, California 91355

Tel 661·309·1010
Fax 661·257·8303

T 110

CERTIFICATE OF CALIBRATION
GAMMA STANDARD SOURCE

Radionuclide:	Eu-152	**Customer:**	AIR FORCE INSTITUTE OF TECHNOLOGY/ENP
Half-life:	4933 ± 11 days	**P.O. No.:**	IA3204PS105/VISA K. POPE
Catalog No.:	GF-152-D	**Reference Date:**	15-Dec-04 12:00 PST
Source No.:	1075-88	**Contained Radioactivity:**	10.14 µCi 375.2 kBq

Physical Description:

A. Capsule type:	D (25.4 mm OD x 6.35 mm THK)
B. Nature of active deposit:	Evaporated metallic salt
C. Active diameter/volume:	5 mm
D. Backing:	Epoxy
E. Cover:	Acrylic

Radioimpurities:

Eu-154 = 0.736% on 15-Dec-04

Method of Calibration:

This source was assayed using gamma ray spectrometry.

Peak energy used for integration:	344.3 keV
Branching ratio used:	0.266 gammas per decay

Uncertainty of Measurement:

A. Type A (random) uncertainty:	± 0.5 %
B. Type B (systematic) uncertainty:	± 3.0 %
C. Uncertainty in aliquot weighing:	± 0.0 %
D. Total uncertainty at the 99% confidence level:	± 3.0 %

Notes:

- See reverse side for leak test(s) performed on this source.
- IPL participates in a NIST measurement assurance program to establish and maintain implicit traceability for a number of nuclides, based on the blind assay (and later NIST certification) of Standard Reference Materials (as in NRC Regulatory Guide 4.15).
- Nuclear data was taken from IAEA-TECDOC-619, 1991.
- This source has a working life of 5 years.

JM Mulhern
Quality Control

23 Nov 04
Date

IPL Ref. No.: 1075-88

Appendix D. Sample MCNP DRF Input File

```
Tosha EXPERIMENT INPUT DECK
c Detector Response Function
c 1.1 billion particles
c cell cards for detector
1 6 -1.05 (7 -8 21 -11):(11 -10 -8):(27 -21 7 -9) IMP:p 1 $ shore70 cover
2 3 -2.699 (30 -27 -7):(27 -12 6 -7):(12 -11 -7) IMP:p 1 $ end cap
3 3 -2.669 (20 -19 1 -5):(19 -14 4 -5):(14 -13 -5) IMP:p 1 $ mount cup
7000 8 -8 (5 -7000 20 -13) IMP:p 1 $ SS
4 5 -2.34 (18 -17 1 -2):(17 29 -28) IMP:p 1 $ Boron contact layer
5 4 -.534 (18 -16 3 -4):(-26 15 -14):(26 -4 25 -24 16 -14)  IMP:p 1 $ Li
6 1 -5.3234 (18 -17 2 -3):(17 -16 -3 28):(16 -15 -26):(-25)  IMP:p 1  $HpGe
7 0 (16 -14 24 -4 26) IMP:p 1 $vacuum space
8 0 (-29):(18 -17 -1):(19 -18 -4):(20 -12 7000 -6):(5 -7000 13 -12) IMP:p 1
9 0 (13 -12 -5):(20 -19 -1):(-20 27 -6) IMP:p 1
c detector box
10 3 -2.669 (30 -27 33 -35 39 -37 7) IMP:p 1
11 3 -2.669 (-30 31 39 -37 33 -34) IMP:p 1
12 3 -2.669 (-30 31 39 -37 36 -35) IMP:p 1
13 3 -2.669 (31 -30 34 -36 -37 38) IMP:p 1
14 3 -2.669 (31 -30 34 -36 -40 39) IMP:p 1
15 3 -2.669 (32 -31 33 -35 39 -37) IMP:p 1
16 2 -.001225 (-30 31 40 -38 34 -36) IMP:p 1
c concrete floor
600 13 -2.2505 (80 -60 50 -51 70 -71) IMP:p 1
c inside air box
22 0 (-50:51:71:-70:61:-80) IMP:p 0
500 2 -0.001225 (10 -51 70 -71 60 -61) IMP:p 1
501 2 -0.001225 (21 -10 70 -71 60 -61 8):(27 -21 70 -71 60 -61 9) IMP:p 1
c 502 2 -0.001225 (27 -21 70 -71 60 -61 9) IMP:p 1
503 2 -0.001225 (50 -27 70 -71 60 -61) #10 #11 #12 #13 #14 #15 #16 #2 IMP:p 1
c end of cell cards

c beginning of surfaces
c cylinders
1 CX .45000 $ coaxial hole (vacuum)
2 CX .45003 $ boron
3 CX 2.4650 $ HPGe
4 CX 2.5000 $ Lithium
5 CX 2.6500 $ Al
7000 cx 2.688 $ SS
6 CX 3.6500 $ Vacuum
7 CX 3.8000 $ Al
```

```
8 CX 4.2699 $ Shore70elastomer
9 CX 5.5699 $ " "
c detector planes (dim. out to end)
10 PX 0.0001 $Shore70elstomer
11 PX -.2686 $ Al
12 PX -.3686 $ Vacuum
13 PX -1.3686 $ Al
14 PX -1.4686 $ Lithium
15 PX -1.5036 $ HPGe end
16 PX -2.2686 $ HPGe to round edge
17 PX -3.4186 $ HPGE top of hole before radius
18 PX -4.4686 $ HPGe bottom of crystal
19 PX -6.1486  $ start Vacuum below crystal
20 PX -6.4686  $ Al mount cup base
21 PX -6.4592  $ Shore70elastomer lip
27 PX -7.0358
c misc. detector parameters
24 TX -2.2686 0 0 1.7 .8 .8 $ Li torus
25 TX -2.2686 0 0 1.7 .765 .765 $HPGe torus
26 CX 1.7 $ torus cutoff cylinder
28 SX -3.4186 .45003 $ sphere radius end of coax HPGE
29 SX -3.4186 .45000 $ Boron radius
c detector case planes
30 PX -7.239 $ inside of front face
31 PX -35.6616 $ inside of back face
32 PX -35.8648 $ outside of back face
33 PZ -14.8000 $ outside bottom
34 PZ -14.5968 $ inside bottom
35 PZ 10.55 $ outside top
36 PZ 10.3468 $ inside top
37 PY 6.2992 $ outside left side
38 PY 6.0960 $ inside left side
39 PY -6.2992 $ outside right side
40 PY -6.0960 $ inside right side
c Room planes
50 PX -131.5
51 PX 131.5
60 PZ -16.2
61 PZ 288.8
70 PY -131.5
71 PY 131.5
80 PZ -46.2
c end of surface
```

```
MODE P
SDEF ERG=D1 Par=2 POS=50.00 0 0 RAD=D2
SI2 0.0 0.15
SI1 L 0.020 $ energy dist.
SP1 D 1.00 $ energy prob.
F8:P 6 $ dep. in cell
e8      0.00     1.e-5    0.001 3198i 3.200 3.30
M1 32000.04p 1 $ HPGe
M2 7000. 0.755636 8000. 0.231475 18000. 0.012889 $air
M3 13000.04p 1 $ Al
M4 3000.04p 1 $ Li
M5 5000.04p 1 $ Boron
M6 1000. -0.143711 6000. -0.856289 $Polyethylene
M7 82000.04p 1 $ Lead
M8 6000. 0.0003 14000. 0.005 15000. 0.000225 16000. 0.00015 &
24000. 0.19 25000. 0.01 26000. 0.701825 28000. 0.0925 $ ss-304
M9 29000. 1 $Copper
c M10 48000. 0.1 50000. 0.133 82000. 0.267 83000. 0.5 $CerroBend
c M11 1000.04p 0.258 6000.04p 0.172 17000.04p 0.570 $ PVC
M12 48000.04p 1 $ Cd
M13 1000.04p 0.0847636 8000.04p 0.604086 11000.04p 0.0094725 &
12000.04p 0.00299826 13000.04p 0.0248344 14000.04p 0.24186 &
19000.04p 0.00685513 20000.04p 0.0204808 &
26000.04p 0.0046495308 $ Los Alamos Concrete
PRINT
dbcn j j 1 100 100000
CUT:P
NPS 1.1E+09
```

Appendix E. Cd-109 Certificate of Calibration File

Isotope Products Laboratories
An Eckert & Ziegler Company

24937 Avenue Tibbitts
Valencia, California 91355

Tel 661•309•1010
Fax 661•257•8303

T-115

CERTIFICATE OF CALIBRATION
GAMMA STANDARD SOURCE

Radionuclide:	Cd-109	**Customer:**	AIR FORCE INSTITUTE OF TECHNOLOGY
Half-life:	462.6 ± 0.7 days	**P.O. No.:**	IA3006PD59
Catalog No.:	GF-109-M	**Reference Date:**	1-Mar-06 12:00 PST
Source No.:	1169-14-2	**Contained Radioactivity:**	100.4 µCi 3715 kBq

Physical Description:

A.	Capsule type:	M (25.4 mm OD x 3.18 mm THK)
B.	Nature of active deposit:	Evaporated metallic salt
C.	Active diameter/volume:	3 mm
D.	Backing:	9.23 mg/cm² kapton
E.	Cover:	0.254 mm aluminized mylar

Radioimpurities:

Zn-65 < 0.0001%; Sb-124 = 0.00019% on 1-Mar-06

Method of Calibration:

This source was assayed using gamma ray spectrometry.

Peak energy used for integration:	88.0 keV
Branching ratio used:	0.0363 gammas per decay

Uncertainty of Measurement:

A.	Type A (random) uncertainty:	± 0.8 %
B.	Type B (systematic) uncertainty:	± 3.0 %
C.	Uncertainty in aliquot weighing:	± 0.0 %
D.	Total uncertainty at the 99% confidence level:	± 3.1 %

Notes:

- See reverse side for leak test(s) performed on this source.
- IPL participates in a NIST measurement assurance program to establish and maintain implicit traceability for a number of nuclides, based on the blind assay (and later NIST certification) of Standard Reference Materials (as in NRC Regulatory Guide 4.15).
- Nuclear data was taken from IAEA-TECDOC-619, 1991.
- This source has a working life of 2.5 years.

Daniel James Van Dalsem
Quality Control

8-Feb-06
Date

IPL Ref. No.: 1169-14

ISO 9001 CERTIFIED

Medical Imaging Laboratory
24937 Avenue Tibbitts Valencia, California 91355

Industrial Gauging Laboratory
1800 North Keystone Street Burbank, California 91504

Appendix F. Co-57 Certificate of Calibration File

Isotope Products Laboratories
An Eckert & Ziegler Company

24937 Avenue Tibbitts
Valencia, California 91355

Tel 661•309•1010
Fax 661•257•8303

T-113

CERTIFICATE OF CALIBRATION
GAMMA STANDARD SOURCE

Radionuclide:	Co-57	**Customer:**	AIR FORCE INSTITUTE OF TECHNOLOGY/ENP
Half-life:	271.79 ± 0.09 days	**P.O. No.:**	IA3006PD33/VISA/J POLLARD
Catalog No.:	GF-057-M	**Reference Date:**	1-Jan-06 12:00 PST
Source No.:	1151-41-2	**Contained Radioactivity:**	52.71 µCi 1950 kBq

Physical Description:

A. Capsule type:	M (25.4 mm OD x 3.18 mm THK)
B. Nature of active deposit:	Evaporated metallic salt
C. Active diameter/volume:	3 mm
D. Backing:	9.23 mg/cm² kapton
E. Cover:	0.254 mm aluminized mylar

Radioimpurities:

Co-56 = 0.0370%; Co-58 = 0.00743% on 1-Jan-06

Method of Calibration:

This source was assayed using gamma ray spectrometry.

Peak energy used for integration:	122.1, 136.5 keV
Branching ratio used:	0.8560, 0.1068 gammas per decay

Uncertainty of Measurement:

A. Type A (random) uncertainty:	± 0.2 %
B. Type B (systematic) uncertainty:	± 3.0 %
C. Uncertainty in aliquot weighing:	± 0.0 %
D. Total uncertainty at the 99% confidence level:	± 3.0 %

Notes:

- See reverse side for leak test(s) performed on this source.
- IPL participates in a NIST measurement assurance program to establish and maintain implicit traceability for a number of nuclides, based on the blind assay (and later NIST certification) of Standard Reference Materials (as in NRC Regulatory Guide 4.15).
- Nuclear data was taken from IAEA-TECDOC-619, 1991.
- This source has a working life of 18 months.

Daniel James Van Dalsem
Quality Control

2-Dec-05
Date

IPL Ref. No.: 1151-41

ISO 9001 CERTIFIED

Medical Imaging Laboratory
24937 Avenue Tibbitts Valencia, California 91355

Industrial Gauging Laboratory
1800 North Keystone Street Burbank, California 91504

Appendix G. Sb-125, Eu-154, and Eu-155 Solution Certificate of Calibration File

...merce
...ige

...tandards
...rector

ID 00211

National Bureau of Standards Certificate

Standard Reference Material 4276

MIXED-RADIONUCLIDE SOLUTION STANDARD
for the
EFFICIENCY CALIBRATION OF GERMANIUM-SPECTROMETER SYSTEMS

Antimony-125-Tellurium-125m
Europium-154
Europium-155

Source identification	SRM 4276-73
Source description	Liquid in NBS borosilicate-glass ampoule(1)*
Solution composition	30 μg Sb^{+3} and 30 μg Eu^{+3} per gram of 4 M hydrochloric acid
Mass	5.446 g
Reference time	1200 EST May 1, 1981

This standard is intended for use in measuring the full-energy-peak efficiencies of spectrometer systems for x and gamma rays from 27 to 1274 keV, provided that the responses to radiations approximately 5 keV apart can be resolved. Emission rates are specified at 18 energies for photon radiations from a mixture of antimony-125-tellurium-125m, europium-154, and europium-155. Uncertainties are estimated and combined at a level corresponding to a standard deviation of the mean, with the intent that the user can propagate this uncertainty along with other uncertainties in the spectrometer calibration.

Table 1 gives the energies, emission rates, and uncertainties for selected radiations. A footnote indicates how emission rates will change with time. If there are any changes in measured emission rates that would correspond to an emission rate 0.5 percent different from that calculated from Table 1, or in measured half lives that would cause a corresponding difference after five years, notification will be sent to purchasers of the standard.

Table 2 lists the estimates of component uncertainties which have been combined in quadrature to give the total uncertainty in each emission rate.

Notes on the use of this standard are appended. One of the tables in the supplemental notes gives relative emission rates for radiations close in energy to the certified radiations; for spectrometer systems of poorer resolution, it may be necessary to use a combined emission rate for some multiple peaks.

This Standard Reference Material was prepared in the Center for Radiation Research Nuclear Radiation Division, Radioactivity Group, D.D. Hoppes, Group Leader.

Washington,D.C. 20234
June, 1981

George A. Uriano, Chief
Office of Standard Reference Materials

*Footnotes on page 4

TABLE 1

X-Ray and Gamma-Ray Energies, Emission Rates per Gram of Solution [2], and Uncertainties for Standard Reference Material 4276

Radionuclide	Photon Energy (keV)	Emission Rate per Gram ($x\ s^{-1}g^{-1}$) or ($\gamma\ s^{-1}g^{-1}$) 1200 EST May 1,1981 *	Total Estimated Uncertainty (%)**
^{125}Sb-^{125m}Te	K_α, 27.4	6.53×10^3	1.3
^{154}Eu-^{155}Eu	K_α, 42.8	4.06×10^3	1.3
^{155}Eu	86.6	2.01×10^3	0.8
^{155}Eu	105.3	1.389×10^3	1.1
^{154}Eu	123.1	5.92×10^3	0.7
^{125}Sb	176.4	7.16×10^2	0.6
^{154}Eu	248.0	1.004×10^3	0.6
^{125}Sb	380.5	1.587×10^2	0.8
^{125}Sb	427.9	3.11×10^3	0.7
^{125}Sb	463.4	1.094×10^3	0.7
^{154}Eu	591.7	7.18×10^2	0.6
^{125}Sb	600.6	1.848×10^3	0.6
^{125}Sb	635.9	1.181×10^3	0.6
^{154}Eu	723.3	2.92×10^3	0.6
^{154}Eu	873.2	1.771×10^3	0.7
^{154}Eu	996.4	1.516×10^3	1.0
^{154}Eu	1004.8	2.63×10^3	0.7
^{154}Eu	1274.4	5.06×10^3	0.6

*Emission rates at later times can be calculated using the decay constants in footnote (3). For the 42.8-keV Gd K_α x rays, the emission rate N_t is given by

$$N_t = N_0 \times 0.71673\ e^{-2.235 \times 10^{-4} t} \times [1 + 0.39523\ e^{-1.777 \times 10^{-4} t}],$$

where N_0 is the emission rate given above and t is the time in days from 1200 EST May 1, 1981.

**Estimated total uncertainties have the significance of one standard deviation of the mean. Components of these estimates are given in Table 2.

(2)

TABLE 2

Estimates of the Component Uncertainties for Photon-Emission-Rate Values for SRM 4276

Photon Energy (keV)	Number of Determinations	TYPICAL UNCERTAINTY COMPONENTS (%)						
		Std. Dev. of the Mean	Efficiency	Peak Analysis	Pile-up Compensation	Geometry	Other*	Overall Uncertainty**
27.4	6	0.3	1.0	0.7	0.3	0.1	0.2	1.31
42.8	6	0.06	1.0	0.7	0.1	0.1	0.5	1.3
86.6	6	0.12	0.65	0.3	0.1	0.1	0.05	0.74
105.3	6	0.09	1.0	0.3	0.1	0.1	0.05	1.1
123.1	6	0.08	0.6	0.4	0.1	0.08	0.05	0.74
176.4	6	0.09	0.5	0.2	0.2	0.1	0.05	0.59
248.0	6	0.04	0.5	0.3	0.1	0.08	0.05	0.60
380.5	6	0.36	0.7	0.2	0.2	0.08	0.05	0.84
427.9	6	0.23	0.7	0.2	0.2	0.08	0.05	0.79
463.4	7	0.22	0.58	0.2	0.2	0.08	0.05	0.69
591.7	6	0.12	0.45	0.3	0.1	0.08	0.05	0.57
600.6	7	0.20	0.42	0.4	0.2	0.08	0.05	0.65
635.9	6	0.19	0.42	0.2	0.2	0.08	0.05	0.55
723.3	6	0.05	0.54	0.2	0.1	0.08	0.05	0.59
873.2	5	0.12	0.63	0.3	0.1	0.08	0.05	0.72
996.4	5	0.11	0.54	0.75	0.1	0.08	0.05	0.94
1004.8	5	0.06	0.54	0.4	0.1	0.08	0.05	0.69
1274.4	5	0.06	0.45	0.1	0.1	0.08	0.05	0.48

*Includes contributions for the half lives for the Te x ray, for the decay schemes for the Gd x ray, as well as source preparation uncertainties.

**Components of the uncertainty have been added in quadrature. This is the overall uncertainty for a typical detector, and some of the values are slightly greater than those given in the last column on Table 1.

FOOTNOTES FOR SRM 4276

(1) Approximately five milliliters of solution. Ampoule specifications:

body diameter	16.5 ± 0.5 mm
wall thickness	0.60 ± 0.04 mm
barium content	less than 2.5 percent
lead oxide content	less than 0.02 percent
other heavy elements	trace quantities

(2) These values are based on gamma-ray spectrometry measurements made at the National Bureau of Standards, which are described in the reference: B.M. Coursey, D.D. Hoppes, and F.J. Schima, "Determination of the Photon Emission Rates of the NBS Long-Lived Mixed-Radionuclide Standard", in Proc. Fifth Symp. X- and Gamma-Ray Sources and Applications, June 10 - 12, 1981, Ann Arbor, Michigan. To be published in Nuclear Instruments and Methods.

(3) The NBS-measured half-life values and computed decay constants are:

	Half Life	Decay Constant
^{125}Sb	2.75 ± 0.02 years	6.901×10^{-4} days^{-1}
^{154}Eu	8.49 ± 0.11 years	2.235×10^{-4} days^{-1}
^{155}Eu	4.73 ± 0.03 years	4.0122×10^{-4} days^{-1}

New 1 June 83 $t_{1/2}$'s for values from NBS

^{125}Sb 1008.7 ± 1.0 DAYS

^{154}Eu 3127 ± 8 DAYS

^{155}Eu 1741 ± 10 DAYS

(4)

Appendix H. Spectra from One Set of Measurements

70560 sec

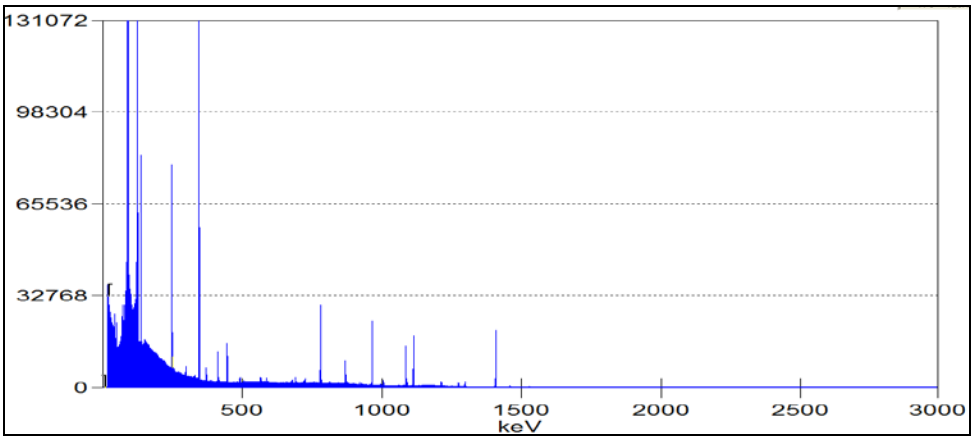

7200 sec

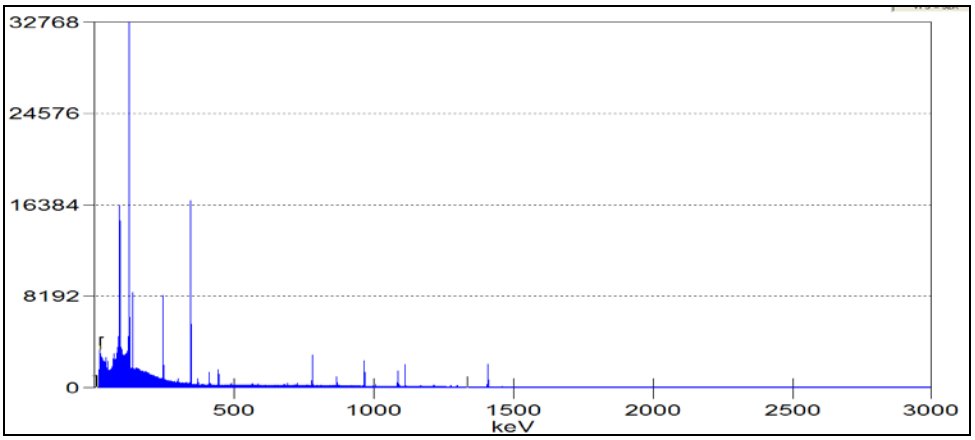

3600 sec

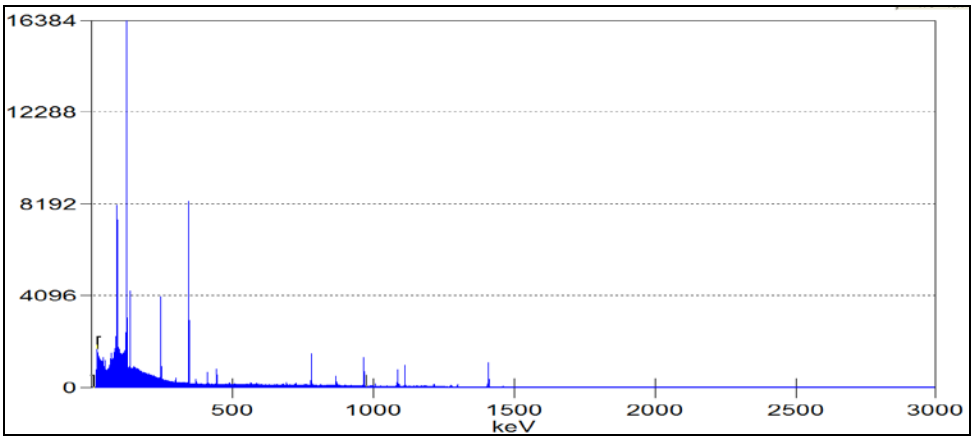

3000 sec

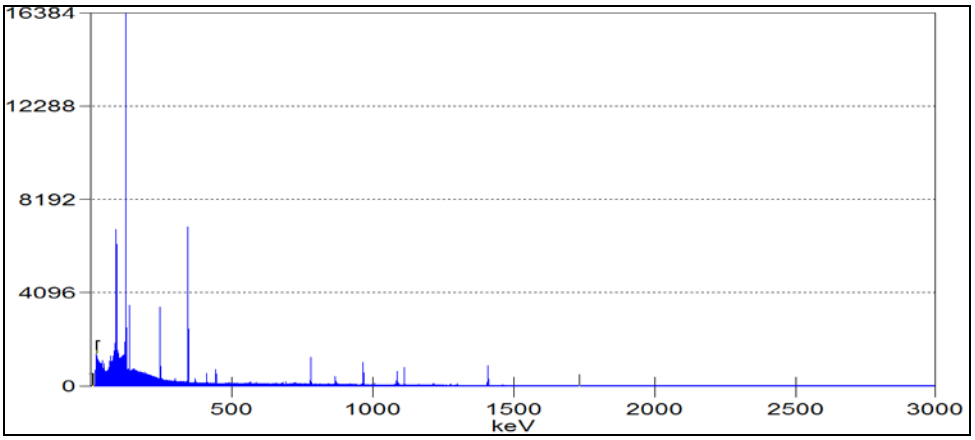

2400 sec

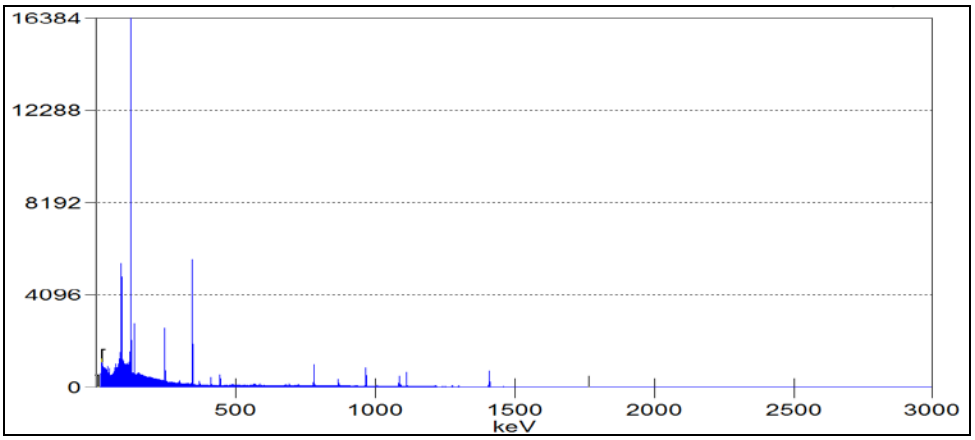

1800 sec

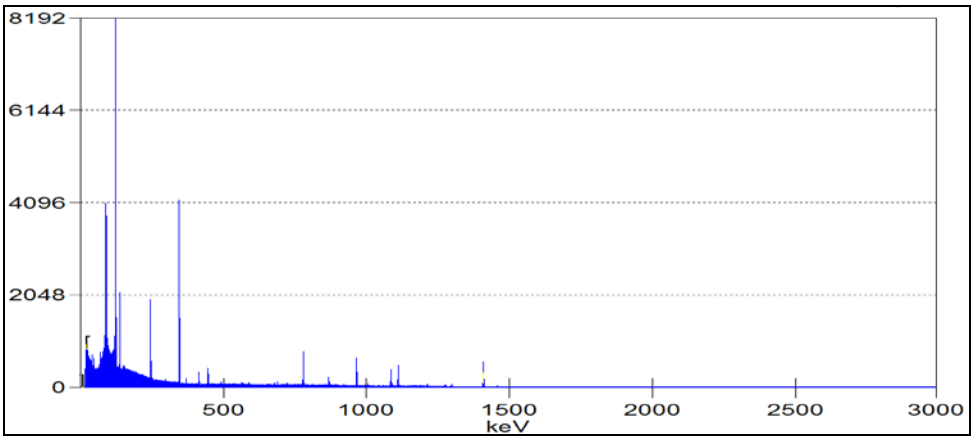

1200 sec

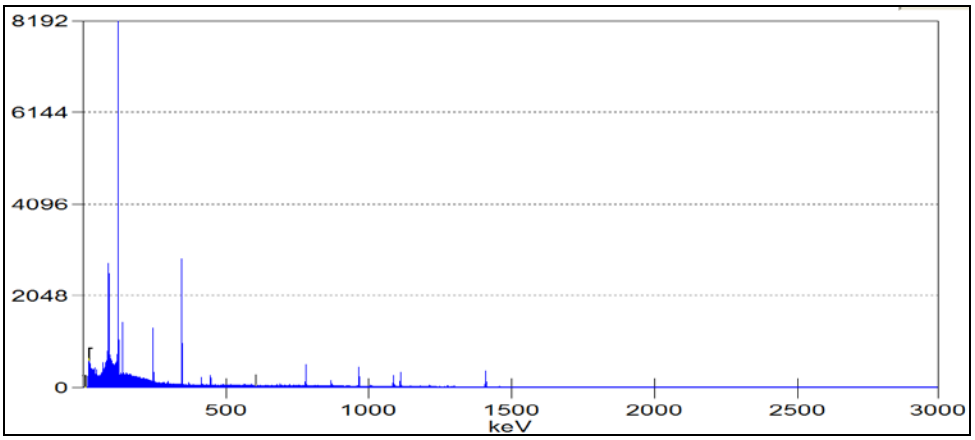

600 sec

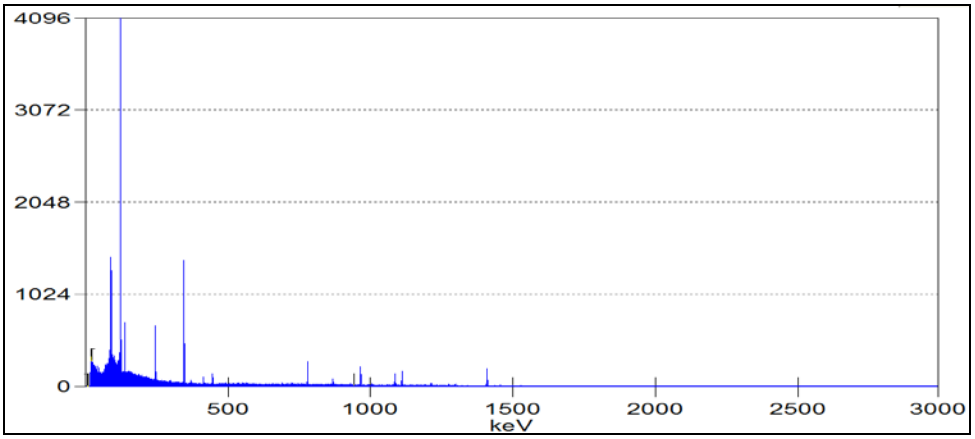

300 sec

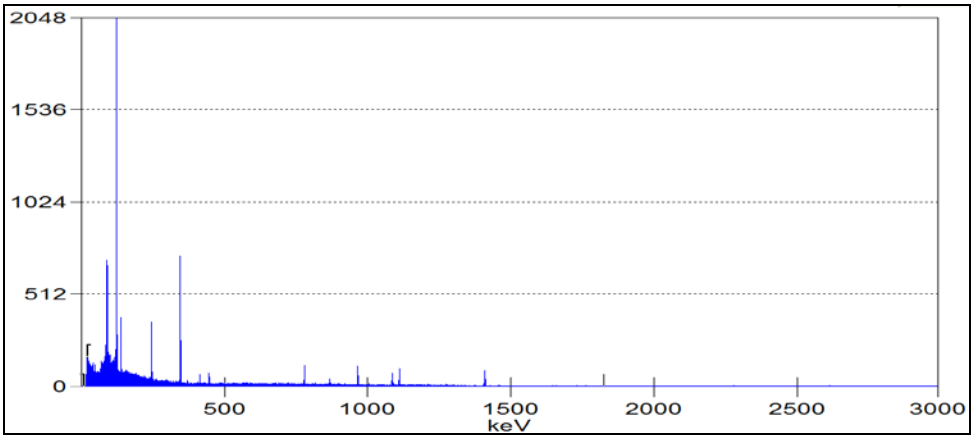

180 sec

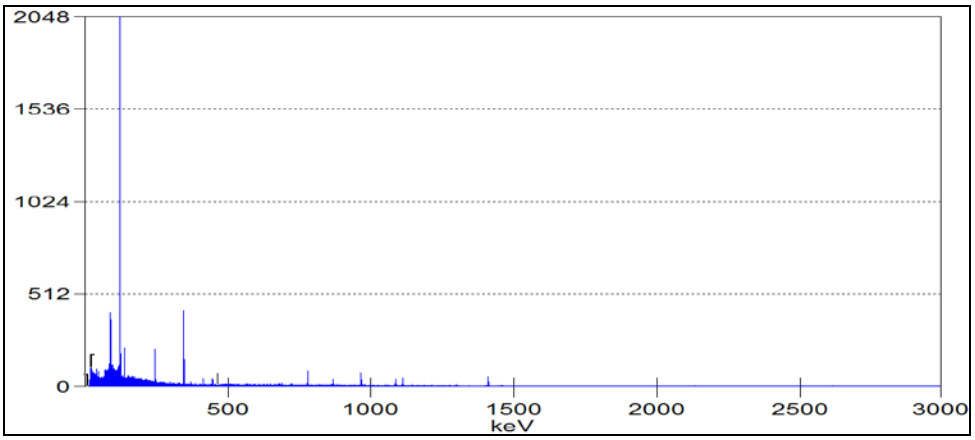

60 sec

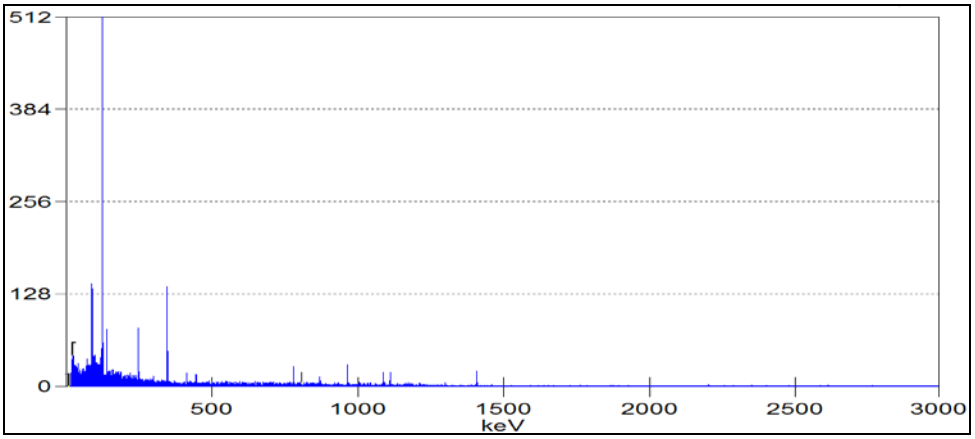

50 sec

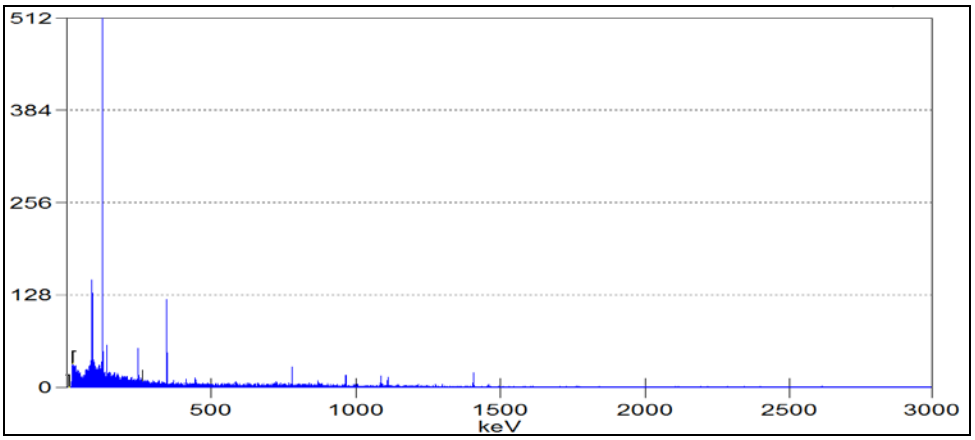

40 sec

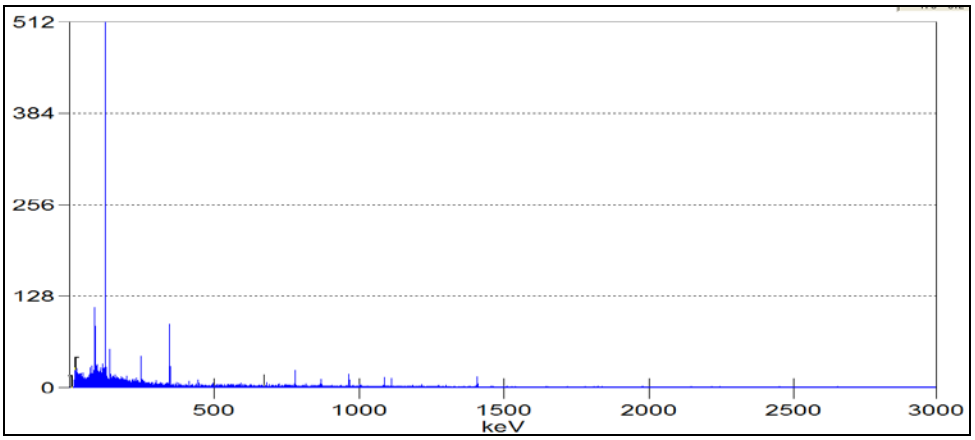

30 sec

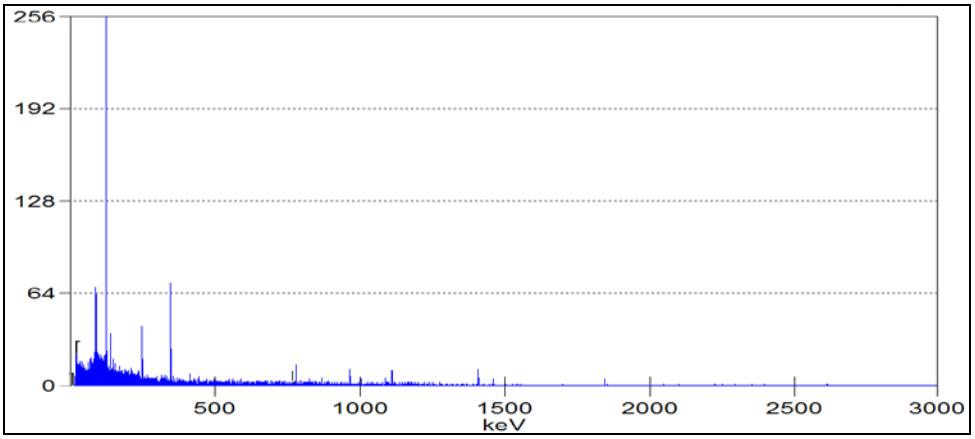

20 sec

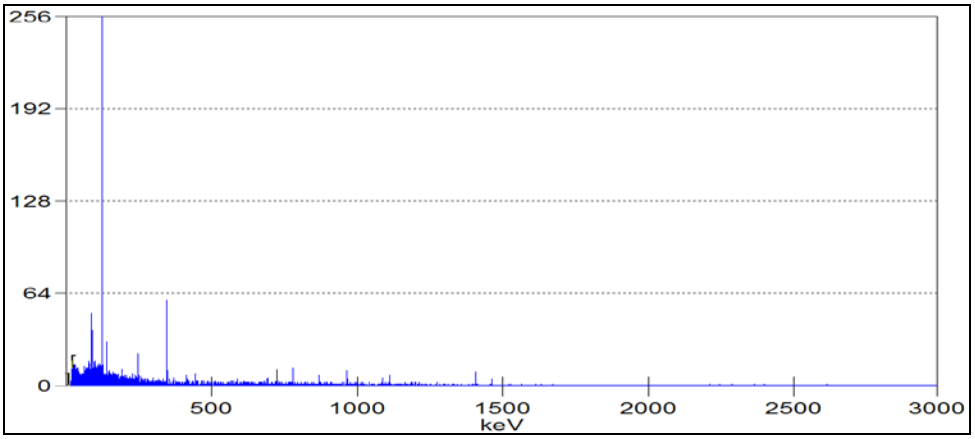

10 sec

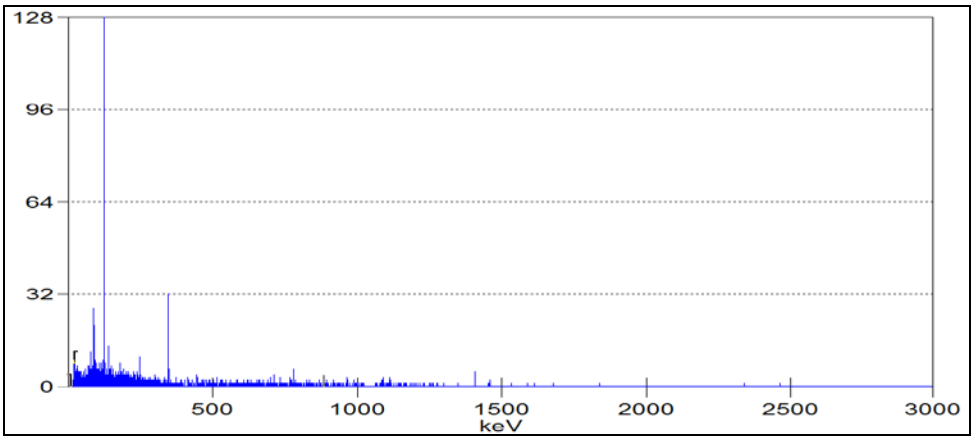

5 sec

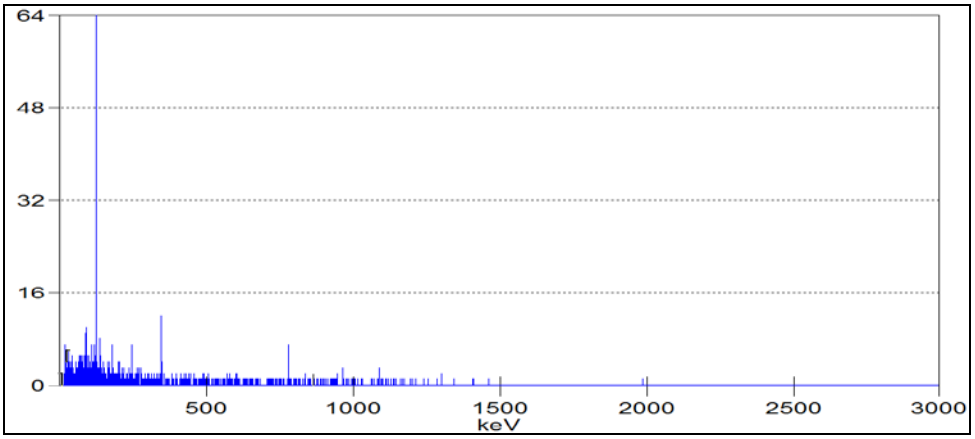

3 sec

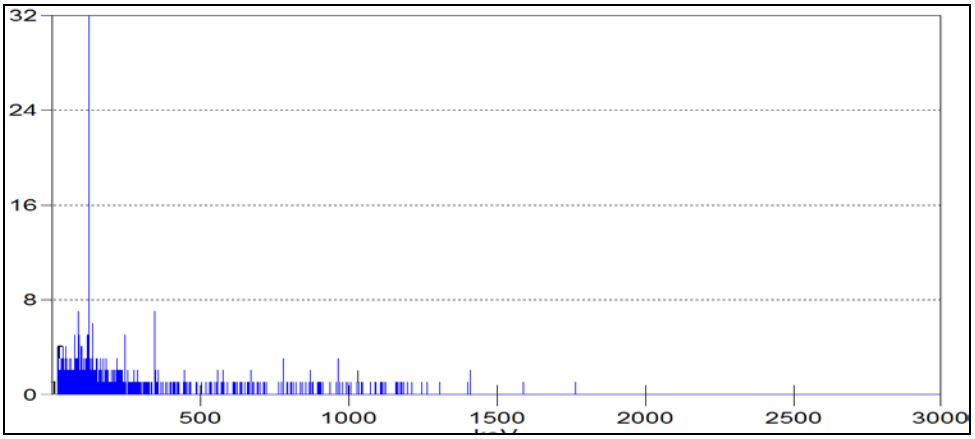

1 sec

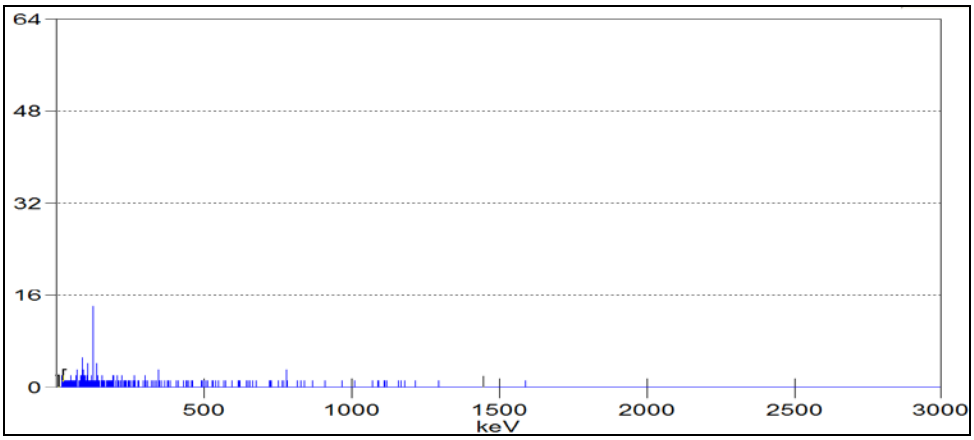

Appendix I. Probability per Decay of Source Gamma Lines

Eu-152 lines (keV)	Probability/Decay
45.40	1.460E-01
121.78	2.840E-01
244.69	7.490E-02
344.27	2.650E-01
411.11	2.210E-02
443.98	2.810E-02
778.89	1.270E-01
867.32	4.160E-02
964.01	1.440E-01
1085.80	9.960E-02
1089.70	1.680E-02
1112.00	1.330E-01
1212.80	1.380E-02
1299.00	1.610E-02
1408.00	2.080E-01

Eu-154 lines (keV)	Probability/Decay
123.07	4.050E-01
247.94	6.600E-02
692.41	1.690E-02
723.30	1.970E-01
756.87	4.330E-02
873.19	1.150E-01
996.32	1.030E-01
1004.80	1.790E-01
1274.50	3.550E-01
1593.00	1.030E-02
1596.50	1.850E-02

Eu-155 lines (keV)	Probability/Decay
45.30	1.290E-02
86.54	3.090E-01

Co-57 lines (keV)	Probability/Decay
122.06	8.560E-01
136.48	1.070E-01

Cd-109 lines (keV)	Probability/Decay
88.04	3.610E-02

Appendix J. Sample Genie™ Peak Analysis Report

Peak Analysis Report 4/3/2009 3:26:44 PM Page 1

****
***** S T A N D A R D V M S P E A K A N A L Y S I S R E P O R T *****
****

Configuration Title: 10dec08_20min_-FCNVT[NEWORTEC]
Spectrum Title:
Peak Analysis Performed on: 4/3/09 3:26:44 PM
Peak Analysis From Channel: 38 To Channel: 8192
Peak Search Sensitivity: 3.30 Gaussian Sensitivity: 15.00
Max Iterations: 10 Fit Singlets: No Critical Level Test: No
Use Fixed FWHM: No FWHM Reject: No FWHM Reject Ratio: 0.00
Peak Fit Engine Name: NDSTD Continuum Type: STEP

	Pk	IT	Energy	Area	Bkgnd	FWHM	Channel	Left	Pw	Cts/Sec	%err	Fit
	1	0	39.66	509	5030	2.01	108.07	101	16	4.3E-001	24.6	0.0
	2	0	45.44	738	4347	1.73	123.87	116	17	6.2E-001	16.2	0.0
M	3	4	66.62	472	6214	3.49	181.81	172	27	4.0E-001	32.1	8.5
m	4	4	68.88	1609	8168	3.58	188.00	172	27	1.4E+000	11.1	8.5
M	5	7	83.47	1523	10871	2.64	227.89	217	48	1.3E+000	14.2	93.3
m	6	7	88.07	15901	13529	3.23	240.48	217	48	1.3E+001	1.7	93.3
	7	0	121.84	67069	11036	1.41	332.86	319	28	5.7E+001	0.5	0.0
	8	0	136.48	4949	5657	1.37	372.89	362	22	4.2E+000	3.1	0.0
M	9	10	245.10	5247	1317	1.45	669.99	659	24	4.4E+000	1.7	2.4
m	10	10	248.27	24	811	1.46	678.65	659	24	2.0E-002	172.0	2.4
	11	0	296.37	294	1427	1.42	810.24	799	22	2.5E-001	23.7	0.0
	12	0	344.68	12259	1267	1.48	942.38	929	26	1.0E+001	1.1	0.0
	13	0	368.27	403	836	1.77	1006.89	995	25	3.4E-001	14.3	0.0
	14	0	411.67	827	826	1.62	1125.60	1114	25	7.0E-001	7.4	0.0
	15	0	444.41	1145	703	1.62	1215.16	1203	24	9.7E-001	5.2	0.0
	16	0	488.28	132	702	2.54	1335.15	1329	23	1.1E-001	37.5	0.0
	17	0	564.79	167	868	1.95	1544.41	1531	26	1.4E-001	34.4	0.0
	18	0	586.26	125	609	1.17	1603.15	1596	20	1.1E-001	35.3	0.0
	19	0	680.45	68	530	2.61	1860.76	1848	18	5.7E-002	57.3	0.0
	20	0	690.16	108	538	0.75	1887.34	1874	19	9.1E-002	37.5	0.0
	21	0	724.25	97	472	1.81	1980.57	1972	16	8.2E-002	38.0	0.0
	22	0	779.56	2482	526	1.73	2131.86	2119	26	2.1E+000	2.7	0.0
	23	0	868.02	677	483	1.92	2373.81	2364	21	5.7E-001	6.9	0.0
	24	0	877.47	223	689	2.33	2399.66	2384	38	1.9E-001	26.6	0.0
	25	0	964.87	2363	393	1.74	2638.73	2622	37	2.0E+000	2.8	0.0
	26	0	1006.15	180	218	2.06	2751.65	2739	21	1.5E-001	16.3	0.0
M	27	9	1086.56	1449	134	2.13	2971.59	2951	43	1.2E+000	3.0	1.2
m	28	9	1090.62	289	135	2.37	2982.68	2951	43	2.4E-001	11.9	1.2
	29	0	1112.75	1901	272	1.93	3043.23	3025	32	1.6E+000	2.9	0.0
	30	0	1214.32	141	190	2.01	3321.03	3306	25	1.2E-001	20.1	0.0
	31	0	1275.82	147	76	2.37	3489.24	3477	25	1.2E-001	13.9	0.0
	32	0	1300.15	173	41	1.98	3555.79	3545	23	1.5E-001	10.2	0.0
	33	0	1408.81	2274	40	2.05	3853.01	3834	33	1.9E+000	2.2	0.0
M	34	3	1528.42	28	0	4.75	4180.18	4163	28	2.3E-002	22.2	0.6
m	35	3	1530.09	23	0	3.15	4184.73	4163	28	1.9E-002	20.8	0.6

M = First peak in a multiplet region
m = Other peak in a multiplet region
F = Fitted singlet

Errors quoted at 1.000 sigma

Appendix K. Sample ASEDRA Peak Analysis Report

1.4088E+03	4.8830E+02
1.2999E+03	3.4361E+01
1.2754E+03	1.6580E+01
1.2139E+03	2.1530E+01
1.1127E+03	4.6082E+02
1.0900E+03	4.5111E+01
1.0867E+03	2.8925E+02
1.0056E+03	4.1037E+01
9.6497E+02	5.5661E+02
8.6809E+02	1.2547E+02
7.7961E+02	6.4534E+02
6.8931E+02	1.6881E+01
4.4435E+02	2.9485E+02
4.1145E+02	2.3201E+02
3.6831E+02	4.2896E+01
3.4455E+02	4.1819E+03
2.9629E+02	2.9479E+01
2.4510E+02	1.1973E+03
1.3652E+02	1.4412E+03
1.2189E+02	2.4358E+04
8.7890E+01	2.3293E+03

Bibliography

[1] Chivers, Daniel H., et al., "Before the Day After: Using Pre-Detonation Nuclear Forensics to Improve Fissile Material Security", *Arms Control Today*, Vol. 38, July/August 2008.

[2] Carchon, R., et al., "Gamma Radiation Detectors for Safeguards Applications", *Instr. and Meth. Phys. Res.* A 579 (2007) 380-383.

[3] Dunlop, William and H. Smith. "Who Did It? Using International Forensics to Detect and Deter Nuclear Terrorism", *Arms Control Today*, Vol. 36, October 2006.

[4] Carter, Ashton B., M. M. May, and W. J. Perry. "The Day After: Action Following a Nuclear Blast in a U.S. City", *The Washington Quarterly*, Vol. 30, Issue 4, pp 19-32, 2007.

[5] Sangsingkeow, P., et al., "Advances in Germanium Detector Technology", Nucl. *Instr. and Meth. Phys. Res.* A 505 (2003) 183-186.

[6] LaVigne, E., G. Sjoden, J. Baciak, and R. Detwiler. "Extraordinary improvement in scintillation detectors via post-processing with ASEDRA—solution to a 50-year-old problem", *Chemical, Biological, Radiological, Nuclear, and Explosives (CBRNE) Sensing IX*, Vol. 6954, April 2008.

[7] Knoll, Glenn F. Radiation Detection and Measurement, 3rd Ed. (2000).

[8] Majer, M., et al., "Effects of near-source photon scattering at the energy of 60 keV". *Nucl. Instr. and Meth. Phys. Res.* A 524 (2004) 227-235.

[9] Majer, M., et al., "Effects of near-source Compton scattering in low-energy gamma-ray spectra", *Nucl. Instr. and Meth. Phys. Res.* A 555 (2005) 243-250.

[10] Uroic, M., M. Majer, S. Pasic, and K. Ilakovac, "Improvements of 60 keV gamma-ray spectrum by reducing scattering", *Nucl. Instr. and Meth. Phys. Res.* A 568 (2006) 772-777.

[11] Plagnard, J., C. Hamon, and M.C. Le´py, "Study of Scattering Effects in Low-Energy Gamma-Ray Spectrometry", *Applied Radiation and Isotopes*, 66 (2008) 769–773.

[12] http://www.ortec-online.com/papers/detective_paper.pdf

[13] MCNP-*A General Monte Carlo N-Particle Transport Code, Version 5, Volume I: Users Guide*, Los Alamos National Laboratory, October 2005.

[14] Vidmar, T., et al., "An intercomparison of Monte Carlo codes used in gamma-ray spectrometry", *Applied Radiation and Isotopes* 66 (2008) 764-768.

[15] Boson, J, G. Agren, and L. Johansson. "A detailed investigation of HPGe detector response for improved Monte Carlo efficiency calculations", *Nucl. Instr. and Meth. Phys. Res.* A 587 (2008) 304-314.

[16] Ayaz-Maierhafer, B. and T. A. DeVol. "Determination of absolute detection efficiencies for detectors of interest in homeland security", *Nucl. Instr. and Meth. Phys. Res.* A 579 (2007) 410-413.

[17] Keyser, R.M. and W. K. Hensley. "Efficiency and Resolution of Germanium Detectors as a Function of Energy and Incident Geometry", *IEEE Transactions on Nuclear Science*, Vol. 1, pp. 375-381 Nov. 2002.

[18] Gutierrez-Villanueva, J.L., et al., "Calibration of a portable HPGe detector using MCNP code for the determination of ^{137}Cs in soils", J. Environ. Radioact. (2008).

[19] Detwiler, R., G. Sjoden, J. Baciak, and E. LaVigne, "Improved Plutonium Identification and Characterization Results with a NaI(Tl) Detector using ASEDRA", *"Optics and Photonics in Global Homeland Security IV"* Proc. SPIE Vol. 6945 (2008).

[20] Genie™ 2000 Spectroscopy System- *Operations Manual*, Canberra Industries, 2001.

[21] Genie™ 2000 Spectroscopy Software – *Customization Tools Manual*, Canberra Industries, 2004.

[22] National Nuclear Data Center Brookhaven National Laboratory, *Evaluated Nuclear Structure Data File*, http://atom.kaeri.re.kr/gamrays.html 2005.

[23] IAEA Evaluated Data – Gamma Rays – Nuclear Training Services http://www.physics.rutgers.edu/~kum/gammas.htm

[24] Lee, Mosung, T.S. Park, and J-K Woo, "Coincidence Summing Effects in Gamma-Ray Spectrometry Using a Marinelli Beaker", *Applied Radiation and Isotopes*, 66 (2008) 799–803.

REPORT DOCUMENTATION PAGE

Form Approved
OMB No. 074-0188

1. REPORT DATE *(DD-MM-YYYY)*	2. REPORT TYPE	3. DATES COVERED *(From – To)*
18-06-2009	Master's Thesis	October 2008 – June 2009

4. TITLE AND SUBTITLE
Effect of Advanced Synthetically Enhanced Detector Resolution Algorithm on Specificity and Sensitivity of Portable High Purity Germanium Gamma Detector Spectra

5a. CONTRACT NUMBER

5b. GRANT NUMBER

5c. PROGRAM ELEMENT NUMBER

6. AUTHOR(S)
Bell, LaTosha M.

5d. PROJECT NUMBER
ENP 08-145, ENP 09-260

5e. TASK NUMBER

5f. WORK UNIT NUMBER

7. PERFORMING ORGANIZATION NAMES(S) AND ADDRESS(S)
Air Force Institute of Technology
Graduate School of Engineering and Management (AFIT/EN)
2950 Hobson Way, Building 640
WPAFB OH 45433-7765

8. PERFORMING ORGANIZATION REPORT NUMBER
AFIT/GNE/ENP/09-J01

9. SPONSORING/MONITORING AGENCY NAME(S) AND ADDRESS(ES)
Dr. Ed Turano
Defense Threat Reduction Agency, Nuclear Technologies Directorate
8725 John J. Kingman Rd, MSC 6201
Fort Belvoir VA 22060
(703) 767-2913, DSN 427-2913

10. SPONSOR/MONITOR'S ACRONYM(S)
DTRA/NTD

11. SPONSOR/MONITOR'S REPORT NUMBER(S)

12. DISTRIBUTION/AVAILABILITY STATEMENT
APPROVED FOR PUBLIC RELEASE; DISTRIBUTION UNLIMITED

13. SUPPLEMENTARY NOTES
This material is declared a work of the U.S. Government and is not subject to copyright protection in the United States.

14. ABSTRACT
The ability to identify special nuclear material is one of the necessary prevention mechanisms for preventing proliferation of special nuclear materials. Additionally, if a nuclear event were to occur, information about the nuclear material used may be extracted from gamma spectra, provided it is obtained quickly and accurately. This can be made possible with the use of the exceptional resolution of the HPGe detector. This experiment applied the Advanced Synthetically Enhanced Detector Resolution Algorithm (ASEDRA) to a portable HPGe detector's spectra, to investigate whether improvements in specificity and sensitivity can be obtained. This method has been used to improve performance of NaI(Tl) spectra. In this work, measurements of Cd-109, Co-57, Eu-152, Sb-125, Eu-154, and Eu-155 spectra were used as ground truth gamma emissions. The HPGe spectra were analyzed using ASEDRA and ORTEC's Genie™, a program used by many in the nuclear weapons community for spectroscopy. Genie™ was used as a benchmark for comparison in this experiment. The number of positive and false positive peaks identified by each program was used for comparison, based on ground truth peaks, which are the thirty-one known peaks based on the sources used in the experiment. The results of this work show that Genie™ always locates more ground truth peaks than ASEDRA and that ASEDRA identifies fewer false positive peaks than Genie™ at all but three of the measurement times. In addition, the performance parameter of Genie™ is higher than ASEDRA at short measurement times, implying that ASEDRA does not provide additional spectral information at shorter measurement times. The application of ASEDRA to experimental spectra does not provide any improvements in specificity or sensitivity, as compared to Genie™.

15. SUBJECT TERMS
Portable High Purity Germanium Detector, HPGe, Advanced Synthetically Enhanced Detector Resolution Algorithm, ASEDRA, specificity and sensitivity, Genie™, MCNP modeling, gamma spectroscopy

16. SECURITY CLASSIFICATION OF:			17. LIMITATION OF ABSTRACT	18. NUMBER OF PAGES	19a. NAME OF RESPONSIBLE PERSON
a.REPORT	b. ABSTRACT	c. THIS PAGE			James C. Petrosky, Assistant Professor (AFIT/ENP)
U	U	U	UU	108	19b. TELEPHONE NUMBER *(Include area code)* (937) 255-6565, ext 4562 James.Petrosky@afit.edu

Standard Form 298 (Rev. 8-98)
Prescribed by ANSI Std. Z39-18